Check for updates

Received: 10 August 2026 | Revised: 28 September 2026 | Accepted: 7 October 2026

DOI: 10.1002/pro.70828

RESEARCH ARTICLE

THE PROTEIN SOCIETY WILEY

Mechanism and regulation of Arabidopsis polyamine acetylation by NATA1 and NATA2

Umar F. Shahul Hameed[1] | **Yann-Ru Lou**[2,3] | **Aleczander Young**[3] | **Jian Yan**[2,4] | **Francisco J Guzmán-Vega**[1] | **Ekaterina Aleksenko**[5] | **Huaiyuan Ma**[1] | **Pierre Briozzo**[5] | **Solange Moréra**[6] | **Georg Jander**[2] | **Stefan T. Arold**[1]

[1]KAUST Center of Excellence for Smart Health, Division of Biomedical Sciences, King Abdullah University of Science and Technology (KAUST), Thuwal, Kingdom of Saudi Arabia

[2]Boyce Thompson Institute, Ithaca, New York, USA

[3]College of Biological Sciences, University of California, Davis, Davis, California, USA

[4]College of Natural Resources and Environment, South China Agricultural University, Guangzhou, China

[5]Université Paris-Saclay, INRAE, AgroParisTech, Institute Jean-Pierre Bourgin for Plant Sciences, Versailles, France

[6]Université Paris-Saclay, CEA, CNRS, Institute for Integrative Biology of the Cell (I2BC), Gif-sur-Yvette, France

Correspondence
Stefan T. Arold, KAUST Center of Excellence for Smart Health, Division of Biomedical Sciences, King Abdullah University of Science and Technology (KAUST), Thuwal 23955-6900, Kingdom of Saudi Arabia.
Email: stefan.arold@kaust.edu.sa

Funding information
US National Science Foundation awards, Grant/Award Numbers: 1121788, 1022017; King Abdullah University of Science and Technology, Grant/Award Number: BAS/1/1056-01-01

Review Editor: Zengyi Chang

Abstract

Polyamines are crucial for sustaining plant growth and stress resilience. Spermine/spermidine N1-acetyl transferases (SSATs) regulate polyamine abundance by catalyzing their N-acetylation, thereby reducing the pool of polyamines and producing other bioactive components. Arabidopsis encodes two SSAT paralogues, N-acetyltransferase activity (NATA) 1 and 2, whose physiological differences and regulatory mechanisms remain poorly understood. Here, we report eight crystal structures of NATA1 and NATA2, providing a detailed view of substrate recognition and conformational dynamics during catalysis. Biophysical analyses reveal that NATA2 is markedly more thermostable than NATA1, suggesting a compensatory role for NATA2 under heat stress. Combining structural and biochemical approaches, we further show that stress-induced acidic metabolites, including glutamate and γ-aminobutyric acid, competitively occupy the NATA active site and collectively attenuate polyamine acetylation. Based on these findings, we propose an autoregulatory mechanism in which stress-associated metabolites jointly inhibit SSAT activity to preserve polyamine pools under adverse conditions, while maintaining basal acetylation capacity. This work clarifies SSAT activity and regulation in Arabidopsis and suggests a previously unrecognized link between stress metabolism and polyamine homeostasis in plants.

KEYWORDS
acCoA, crystallography, metabolite, non-proteinogenic amino acid, regulation, stress

Umar F. Shahul Hameed and Yann-Ru Lou contributed equally to this study.

This is an open access article under the terms of the Creative Commons Attribution-NonCommercial-NoDerivs License, which permits use and distribution in any medium, provided the original work is properly cited, the use is non-commercial and no modifications or adaptations are made.
© 2026 The Author(s). *Protein Science* published by Wiley Periodicals LLC on behalf of The Protein Society.

1 | INTRODUCTION

Polyamines are abundant nitrogen-containing metabolites that mediate a wide variety of physiological functions in eukaryotes, bacteria, and archaea. In higher plants, the most common polyamines are the diamines putrescine and cadaverine, the triamine spermidine, and the tetraamine spermine (Kim et al. 2014; Nahar et al. 2016; Regla-Márquez et al. 2016; Sobieszczuk-Nowicka 2017; Takahashi et al. 2018) (Figure 1a). These compounds play a central role in many aspects of plant physiology by influencing transcription, RNA modification, protein synthesis, enzyme activity, and signaling pathways (Evans and Malmberg 1989; Galston et al. 1997; Kusano et al. 2007; Kusano et al. 2008; Sagor et al. 2015; Takahashi and Kakehi 2010; Wimalasekera et al. 2011). In most plants, putrescine, the precursor for the synthesis of higher-order polyamines, is synthesized from arginine in two parallel pathways involving arginine decarboxylase, or *via* the non-proteinogenic amino acid *L*-ornithine (hereafter referred to as ornithine for simplicity), through the ornithine decarboxylase (Figure 1a) (Bagni and Tassoni 2001; Galston and Sawhney 1990). However, ornithine decarboxylase is absent in the model plant *Arabidopsis thaliana* (Arabidopsis) (Hanfrey et al. 2001).

Polyamine abundance is regulated through import, export, synthesis, degradation, and chemical modification (Rhee et al. 2007; Zahedi et al. 2022). Spermidine/spermine N^1-acetyltransferases (SSATs) are GCN5-related *N*-acetyltransferases (GNATs) that use acetyl-coenzyme A (acCoA) as a cofactor to transfer an acetyl to the terminal amino group of polyamines, thus reducing the active pool of polyamines. SSATs have been identified in all kingdoms, including bacteria, protozoans, animals, and plants (Pegg 2008). Polyamine acetylation can also create compounds with new functions and, despite being widely viewed as accumulative products, acetylated polyamines can influence plant metabolism by acting as pathway intermediates that facilitate turnover and translocation of polyamines (Moschou et al. 2012; Tavladoraki et al. 2012). Acetylated polyamines, suggestive of SSAT activity, have been identified in several plant species (Bagni and Tassoni 2001; Fliniaux 2004; Hennion et al. 2012; Lou et al. 2016; Mesnard et al. 2000; Tavladoraki et al. 2012). In Arabidopsis, N^1-acetylspermidine was reported to be as abundant as spermidine in both roots and aboveground tissue (Kamada-Nobusada et al. 2008).

Three-dimensional (3D) structures of SSATs from bacteria, animals, and plants have been deposited in the Protein Data Bank (PDB), but analyses have only been published for those from mouse, human, and the moss *Physcomitrium patens* (Table S1, Supporting Information) (Bělíček et al. 2023; Bewley et al. 2006; Han et al. 2006; Hegde et al. 2007; Montemayor and Hoffman 2008). All SSATs consist of a central β-sheet flanked by helices and form an intertwined obligate dimer through large surface contacts and arm exchange of the *N*-terminal β-strand. Differences between SSAT structures in the free form and bound to cofactors and/or substrates (Table S1) suggest that catalysis involves conformational changes. So far, these structural transitions have not yet been described for the same protein, precluding a precise analysis of structural transitions and their role in catalysis.

Plant SSATs distinguish themselves from animal and bacterial enzymes by a 35-amino acid insert (Figure S1a). In the only SSAT 3D structure reported with this insert, from *P. patens* (Bělíček et al. 2023), it forms an additional β-strand and a loop, with the latter being partially disordered in the crystal structure (Figure S1b). The proximity of the additional β-strand to the cofactor binding site suggests that the insert affects catalysis (Bělíček et al. 2023) but the nature of the effect remains unclear. Indeed, the presence of the plant insert does not correlate with the catalytic rate or substrate preference of the enzyme (Bělíček et al. 2023).

SSATs generally display low turnover rates and a broad substrate profile, ranging from diamines to spermine, also including 1,3-diaminopropane and the non-proteinogenic amino acids ornithine and thialysine (Adio et al. 2011; Jammes et al. 2014; Lou et al. 2016; Mattioli et al. 2022). Nonetheless, several studies show different substrate preferences for some SSATs. These differences in substrate preference were apparent not only between kingdoms but also between species within kingdoms. For example, the plant SSATs from moss, maize, and Arabidopsis were shown to acetylate a range of polyamines, including 1,3-diaminopropane, putrescine, spermidine, and spermine, as well as the precursor amino acid ornithine (Bělíček et al. 2023). However, the substrate preferences differed significantly between plant species, among different parts of the same plant, and depending on whether plants were subjected to osmotic stress or water stress (Sen et al. 2018). Moreover, differences were also observed among paralogues from the same species. Human SSAT2, for example, was reported to acetylate thialysine rather than spermine or spermidine, whereas both of these polyamines were good substrates for human SSAT1 (Coleman et al. 2004; Della Ragione and Pegg 1983; Hegde et al. 2007; Pegg 2008). As an explanation, it was suggested that the polyamine processing profile is dependent on small changes in the protein active site and surrounding areas, allowing polyamine acetylation to be species-specific (Mattioli et al. 2022). Yet, even for the same SSAT, different researchers observed markedly different substrate preferences, suggesting that catalysis can significantly be affected by (unidentified) experimental factors. For instance, the best substrate for the Arabidopsis SSAT *N*-acetyltransferase activity 1 (NATA1; At2g39030) was reported to be either ornithine, thialysine, or putrescine (Adio et al. 2011; Jammes et al. 2014; Lou et al. 2016).

1469896x, 2026, 12, Downloaded from https://onlinelibrary.wiley.com/doi/10.1002/pro.70828 by Portail BibCNRS INSB, Wiley Online Library on [06/11/2026]. See the Terms and Conditions (https://onlinelibrary.wiley.com/terms-and-conditions) on Wiley Online Library for rules of use; OA articles are governed by the applicable Creative Commons License

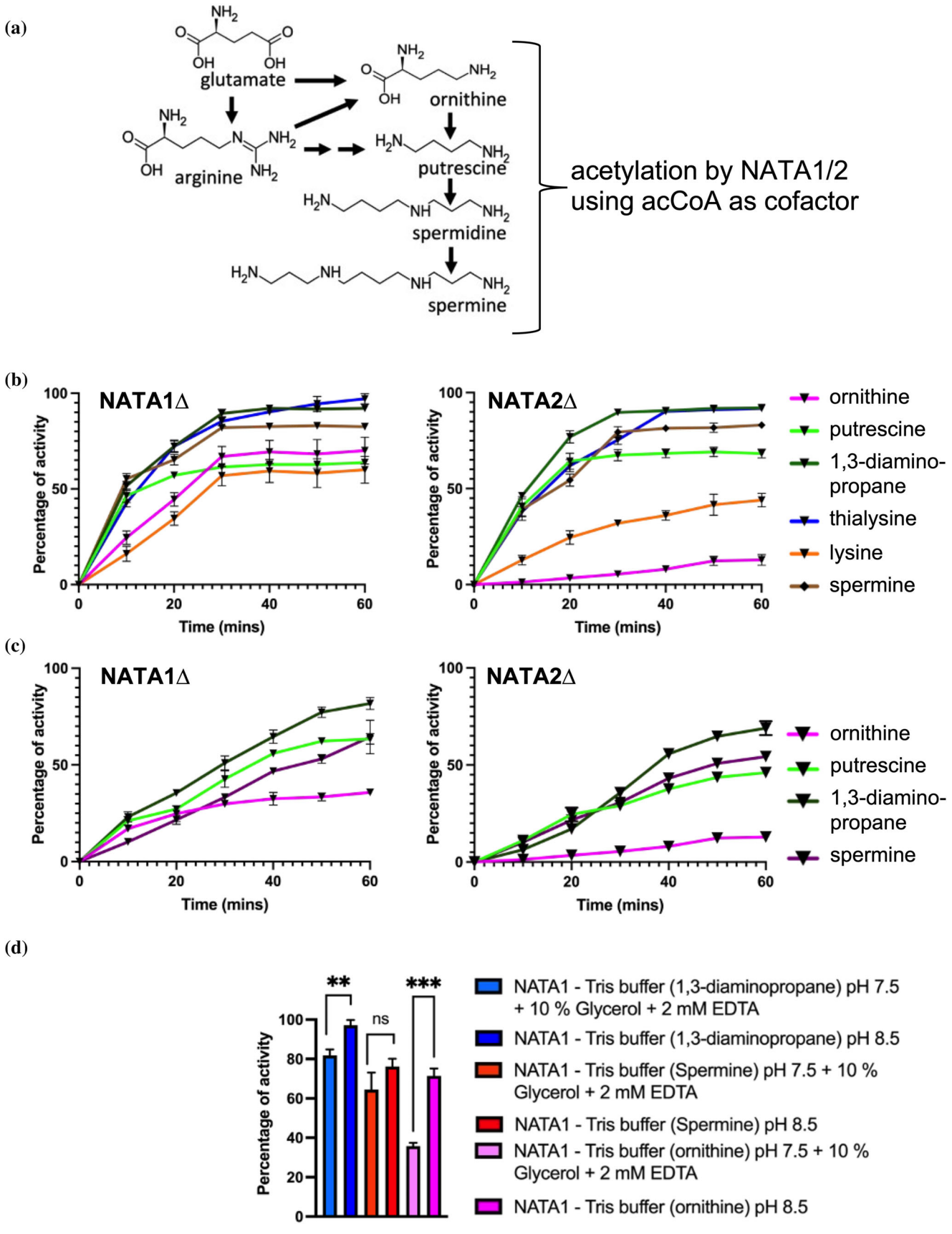


FIGURE 1 Legend on next page.

1469896x, 2026, 12, Downloaded from https://onlinelibrary.wiley.com/doi/10.1002/pro.70828 by Portail BibCNRS INSB, Wiley Online Library on [06/11/2026]. See the Terms and Conditions (https://onlinelibrary.wiley.com/terms-and-conditions) on Wiley Online Library for rules of use; OA articles are governed by the applicable Creative Commons License

Although it is expected that the activity of SSATs is tightly controlled, the basis for this regulation remains poorly defined. In *P. patens*, SSAT is not significantly upregulated under various abiotic stresses (Bělíček et al. 2023), whereas the Arabidopsis *NATA1* expression is upregulated by a variety of stresses, including cold, salinity, drought, wounding, as well as addition of jasmonate, cytokinins, and polyamines (Adio et al. 2011; Jammes et al. 2014; Lou et al. 2016; Mattioli et al. 2022).

A gene duplication event in Arabidopsis and closely related species led to the presence of two *NATA* genes, which encode proteins with approximately 80% amino acid sequence identity (Lou et al. 2016). Unlike *NATA1*, *NATA2* (At2g39020; likely the evolutionarily ancestral gene) was not upregulated by cytokinins and polyamines (Lou et al. 2016; Mattioli et al. 2022). The selective advantage of the *NATA* gene duplication in Arabidopsis, and the biological role of NATA2, remain unclear. Indeed, and surprisingly, the deletion of *NATA1* increases both growth and pathogen resistance of Arabidopsis (Lou et al. 2016), in line with the importance of polyamines for growth and as a substrate for defence assosiated H2O2 production (Yoda et al. 2006: Yoda et al. 2009). The upregulation of *NATA1* in Arabidopsis under conditions where SSAT activity is unfavorable, and the presence of a second highly similar gene are intriguing. Moreover, considering that the catalytic activity of NATA1 and NATA2 on polyamines is generally relatively low and that there are also other pathways for polyamine catabolism (through copper-containing amine oxidases (CuAOs) and flavin-containing polyamine oxidases [polyamineOs]) (Tavladoraki et al. 2016: Yoda et al. 2006), it is unclear how important NATA1 and NATA2 are for plant growth.

Here, we combined structural, biochemical, and *in planta*analyses to elucidate the regulation and biochemical differences between NATA1 and NATA2 in Arabidopsis. Based on these results, we propose the concept of a metabolite-based autoregulatory mechanism that allows selective attenuation of SSAT activity under biotic and abiotic stress.

2 | RESULTS

2.1 | NATA1 and NATA2 have a similar broad substrate preference in vitro

Previously published investigations of the *in planta* substrate preference of NATA1/2, and SSATs more generally, produced diverging or contradictory results, suggesting the action of unidentified additional factors *in planta* (e.g., Adio et al. 2011; Jammes et al. 2014; Lou et al. 2016). Therefore, we started by establishing the substrate profiles under controlled in vitro conditions using *Arabidopsis* NATA1 and NATA2 proteins that were recombinantly expressed in *E. coli*. We produced and purified full-length NATA2, as well as NATA1 and NATA2 constructs where we deleted the flexible *N*-terminal extension (residues 1–18 and 1–29, respectively; named NATA1Δ and NATA2Δ). Due to their higher solubility we used NATA1Δ and NATA2Δ for catalytic assays.

Previous work showed that NATA2 displays optimal catalytic activity at pH 8.5–9.5, consistent with the preference for mildly basic conditions reported for other transaminases (Mattioli et al. 2022; Xiang et al. 2022). When assayed in 50 mM Tris–HCl pH 8.5, 150 mM NaCl (hereafter *Tris8.5*) at 25°C, NATA1Δ exhibited its highest relative activity toward thialysine, 1,3-diaminopropane, and spermine, with only slightly lower activity on ornithine, putrescine, and lysine (Figure 1b and Tables 1 and 2). NATA2Δ displayed a largely similar substrate preference profile, except for ornithine, which was acetylated only at very low levels. This broad substrate preference was not specific to this alkaline buffer, because similar broad acetylation profiles, including the poor catalysis of ornithine by NATA2, were observed at a neutral pH (100 mM Tris–HCl, pH 7.5, 2 mM EDTA, and 10% glycerol; abbreviated as *Tris7.5*, at 25°C) (Figure 1c), albeit with an overall reduction in catalytic efficiency (Figure 1d). We conclude that in vitro, NATA1, and NATA2 have a similar broad substrate usage.

2.2 | NATA1 and NATA2 are structurally highly similar

To investigate the molecular basis for the observed properties of NATA1 and NATA2, we obtained a total of eight different crystal structures at resolutions between 1.1 and 2.0 Å, three for NATA1Δ, four for NATA2Δ, and one for the full-length NATA2, featuring different cofactors, substrates, and conformations (Tables S1 and S2).

In all structures, the catalytic domains of NATA1 (residues 22–227) and NATA2 (residues 29–236) adopt the same intertwined α/β dimer structure as observed for the bacterial, animal, and moss SSAT enzymes with a global RMSD of 2.4 Å (Figures 2a and

FIGURE 1 NATA1Δ and NATA2Δ substrate profiles. (a) Simplified schematic summary of the biosynthesis pathways of ornithine, putrescine, spermidine, and spermine, which are acetylated by NATA1 and NATA2 using acCoA as a cofactor. (b) Catalytic activity of NATA1Δ (left) and NATA2Δ (right) on their substrates measured in buffer *Tris8.5* at 25°C and (c) in buffer *Tris7.5* at 25°C. Concentrations of substrate and acCoA were 5 and 0.5 mM, respectively. Protein concentrations were 3 μM. Data in panels (b, c) are presented as mean ± SEM from three independent replicates. (d) Comparison of the catalytic activity of NATA1Δ against its substrates in the buffer *Tris8.5* and *Tris7.5 + 10% glycerol* at 25°C. Data are shown as mean ± SEM from three independent replicates, and statistical comparisons were performed using a one-way ANOVA (*$p < 0.05$; **$p < 0.01$; ***$p < 0.001$).

1469896x, 2026, 12, Downloaded from https://onlinelibrary.wiley.com/doi/10.1002/pro.70828 by Portail BibCNRS INSB, Wiley Online Library on [06/11/2026]. See the Terms and Conditions (https://onlinelibrary.wiley.com/terms-and-conditions) on Wiley Online Library for rules of use; OA articles are governed by the applicable Creative Commons License

TABLE 1 Relative activity of NATA1Δ and NATA2Δ against substrates.

Relative activity (%)			
Substrate	**NATA1**	**NATA2**	**NATA2 45°C**
Thialysine	97.12 ± 2.67	91.79 ± 1.21	93.25 ± 4.31
1,3-Diaminopropane	92.12 ± 1.67	92.12 ± 1.61	97.45 ± 2.16
Spermine	82.60 ± 0.79	83.13 ± 1.52	97.80 ± 2.12
Putrescine	63.79 ± 1.07	68.28 ± 2.27	76.75 ± 5.99
Ornithine	70.04 ± 7.04	12.87 ± 2.79	67.20 ± 5.63
Lysine	60.04 ± 7.03	44.04 ± 3.50	63.15 ± 2.35

Note: Measurements were carried out in *Tris8.5* buffer at 25 and 45°C.

TABLE 2 Catalytic parameters for recombinant NATA1Δ and NATA2Δ.

	NATA1			NATA2			NATA2 45°C		
Ligand	K_m (mM)	K_{cat} (s^{-1})	K_{cat}/K_m (s^{-1} mM^{-1})	K_m (mM)	K_{cat} (s^{-1})	K_{cat}/K_m (s^{-1} mM^{-1})	K_m (mM)	K_{cat} (s^{-1})	K_{cat}/K_m (s^{-1} mM^{-1})
Thialysine	0.54 ± 0.13	2.04 ± 0.20	3.78	0.33 ± 0.08	2.20 ± 0.10	6.67	0.32 ± 0.05	3.14 ± 0.19	9.82
1,3-Diaminopropane	0.44 ± 0.12	1.59 ± 0.08	3.61	0.37 ± 0.07	1.46 ± 0.07	3.94	0.22 ± 0.04	1.65 ± 0.08	7.5
Spermine	2.26 ± 0.50	1.56 ± 0.10	0.69	1.62 ± 0.35	1.49 ± 0.08	0.92	0.67 ± 0.13	1.31 ± 0.07	1.96
Putrescine	1.90 ± 0.42	1.11 ± 0.12	0.59	2.29 ± 0.48	1.04 ± 0.07	0.45	1.17 ± 0.31	1.00 ± 0.08	0.85
Ornithine	4.04 ± 0.82	0.64 ± 0.05	0.16	N.D.	N.D.	N.D.	1.73 ± 0.42	0.45 ± 0.13	0.26
Lysine	12.70 ± 3.52	0.58 ± 0.09	0.05	9.48 ± 2.53	0.45 ± 0.10	0.05	5.68 ± 1.25	0.63 ± 0.06	0.11

Note: Measurements were carried out in the *Tris8.5* buffer at 25 or 45°C. N.D. (not determined) indicates that the enzymatic activity was too low to allow accurate quantification.

S1b). The ∼35-residue plant-specific insertion forms an additional β-strand (residues 101–105 and 109–113 for NATA1 and NATA2, respectively) and a short α helix (residues 115–119 and 123–127) similarly to what was observed for *P. patens* SSAT (Bělíček et al. 2023). Structural superposition with bacterial and animal SSAT homologs revealed substantial divergence within this insertion region, with a local RMSD of 7.65 Å (Figures 2a and S1). The remaining insert residues form a loop from which F98, F101, and I111 bind to residues F72, F78, and Y159 of the NATA1 core. These interactions are conserved in NATA2, where they occur between F106, F109, and I119 and F79, F85, and Y167 (Figure S2a). The structure of the unattached part of the loop varies between all the protein chains and lacks continuous electron density in most monomers, suggesting flexibility. In one of the two molecules of the asymmetric unit of the NATA2Δ structure bound to di-CoA, the additional β-strand region (residues 114–109) was displaced by 5–7 Å, losing its secondary structure (Figure S2b). This conformation likely resulted from the insertion of the *C*-terminal helix of a neighboring molecule, suggesting that the structure of the plant-specific insert at this position can accommodate ligands. In full-length NATA2, only residues 20–29 of the *N*-terminal extension were visible. These residues were loosely associated with the cofactor binding site of a crystallographically related NATA2 molecule, as illustrated by their above-average B-factors, supporting that the residues preceding the NATA2Δ core are flexible. The core domains of NATA2 and NATA2Δ were identical within measurement errors (RMSD = 0.75 Å), confirming that the *N*-terminal extension does not affect the structure of the catalytic domain.

Across all structures containing (ac)CoA, the α and β phosphates of the cofactor were coordinated in an identical manner by the backbone nitrogens of the P-loop and the following helix (residues 161–166 and 169–174 for NATA1 and NATA2, respectively). In contrast, the positions of the remaining portions of the cofactor varied depending on the structural context. Compared to other known SSAT structures, the P-loops of NATA1 and NATA2 contain an additional arginine (R161 and R169, respectively) which contributes to coordinating the 3′ phosphate in some structures. This arginine is present only in higher plants such as Arabidopsis and maize, but absent in moss, human, or *Pseudomonas aeruginosa* SSATs, and may introduce species-specific differences in cofactor-binding dynamics (Figure S2c).

2.3 | NATA1 and NATA2 crystal structures show open and closed conformations

NATA2 structures revealed two distinct conformations. (1) An open state, in which both the substrate and cofactor binding sites are solvent-exposed. This

1469896x, 2026, 12, Downloaded from https://onlinelibrary.wiley.com/doi/10.1002/pro.70828 by Portail BibCNRS INSB, Wiley Online Library on [06/11/2026]. See the Terms and Conditions (https://onlinelibrary.wiley.com/terms-and-conditions) on Wiley Online Library for rules of use; OA articles are governed by the applicable Creative Commons License

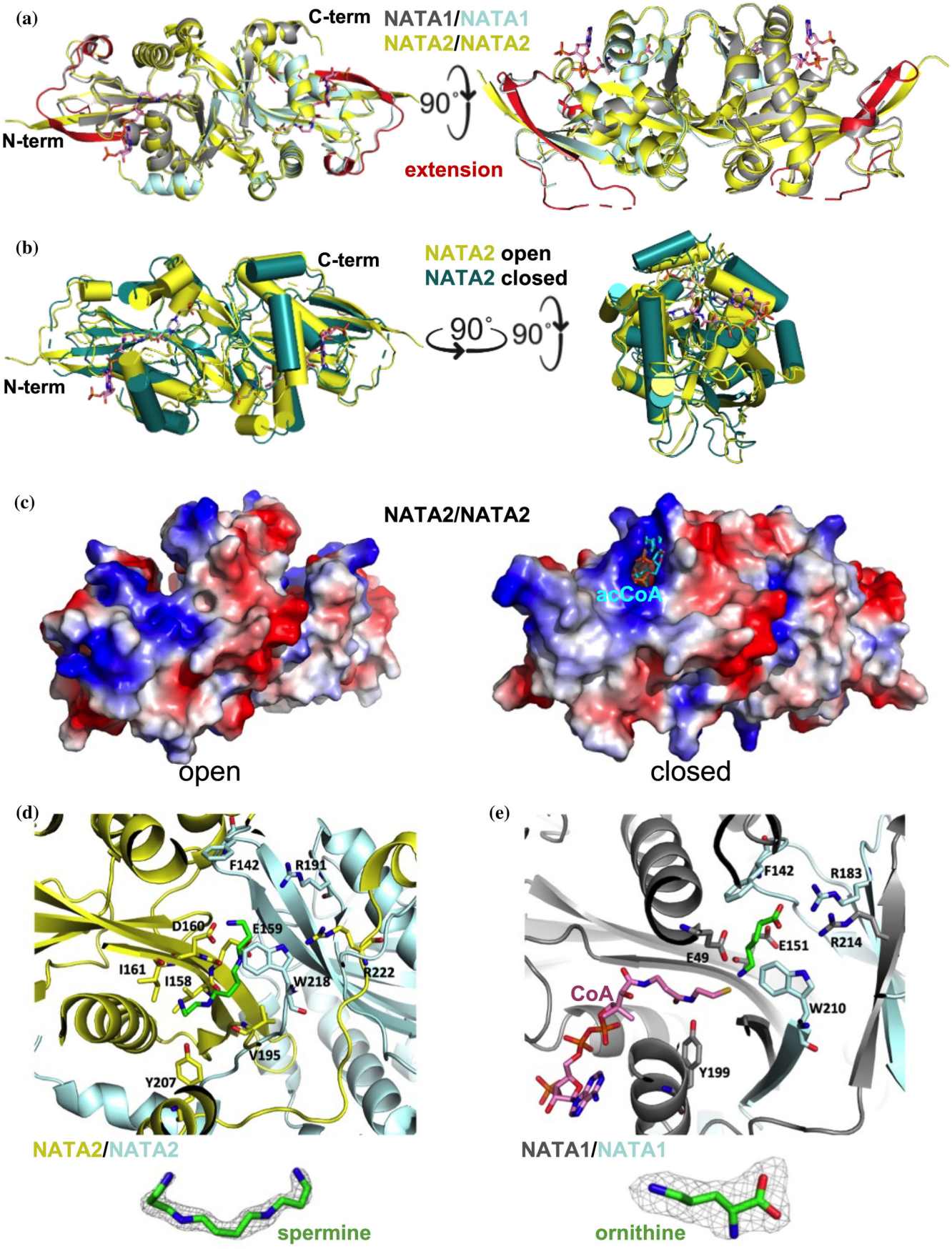


FIGURE 2 Legend on next page.

1469896x, 2026, 12, Downloaded from https://onlinelibrary.wiley.com/doi/10.1002/pro.70828 by Portail BibCNRS INSB, Wiley Online Library on [06/11/2026]. See the Terms and Conditions (https://onlinelibrary.wiley.com/terms-and-conditions) on Wiley Online Library for rules of use; OA articles are governed by the applicable Creative Commons License

conformation was observed in full-length NATA2, apo-NATA2Δ, and in NATA2Δ complexes with spermine or di-CoA. (2) A closed state, in which the substrate-binding pocket and the acetyl-bearing tail of acCoA are occluded by surrounding protein elements. This state was captured in NATA2Δ structures bound to acCoA or HEPES (Figure 2b,c). All NATA1Δ structures adopted closed conformations, although the acCoA-only complex displayed a slightly more open arrangement compared to structures bound to CoA together with substrates. In the closed state of both NATAs, the substrate-binding site and the acetyl-containing portion of acCoA become fully enclosed within a tunnel that spans the protein core (Figure 2c). The substrate-facing entrance of this tunnel is considerably narrower in the closed NATA1 and NATA2 structures than in closed human SSATs.

The transition from open to closed involves a coordinated pinching movement of the NATA2 regions 39–82 and 196–201 (corresponding to NATA1 residues 32–74 and 188–193), located on opposite sides of the central β-sheet. The resulting motion closes over the substrate and catalytic site. In addition, an outward shift and partial restructuring of residues 161–188 (NATA1 residues 153–180) remodels the binding region for the diphosphate moiety of acCoA (Figure 2b). In the open NATA2Δ structure with spermine (PDB 8XJB), spermine is lodged in the middle of the catalytic site, on the side of the central β-sheet. In the open full-length NATA2 structure (PDB 8RMZ), an ethanediol molecule is found in the same place, mimicking the substrate. This substrate position is partially overlapping with the acCoA binding site in closed structures (Figure 2d,e). Hence, upon acCoA binding and NATA2 closure, spermine would be pushed toward the back of the substrate-binding site, near to the center of the NATA protein dimer.

It is tempting to speculate that acCoA binding promotes the closed state, at least in NATA1, possibly by acCoA-initiated restructuring of residues 153–180. In support, most of our NATA1 or NATA2 cofactor-bound structures were in a closed state (Table S1). However, not all cofactor-associated structures of SSATs are closed. For instance, NATA2Δ in complex with the di-CoA adopts the open form, as do some (ac)CoA-bound molecules from mouse, human, and moss structures (PDB 3BJ8, 2B4B chain B, and 7ZHC chain B, respectively). In all these open structures, the CoA diphosphates are bound in the same position as in the closed form, but the adenosine is curled back in the active site (through hydrophobic contacts with helix α1), a position that would clash with the closed form (where the adenosine and 3′ phosphate are extending outside the pocket; Figure S5a). Conversely, the *P. aeruginosa* SSAT crystal structure (PDB 2FE7) shows a closed conformation even in the absence of CoA. We concluded that, although cofactor binding may favor the closed form, the joint presence of the substrate may promote it further. Moreover, the conformation is likely influenced by the crystallization conditions and crystal packing, and the energetic barrier between open and closed structures may be low.

Based on the structural data, we propose that the substrate first binds centrally (e.g., spermine contacting D160 and W218′). Binding of the acCoA diphosphates to NATA in the presence of the substrate may promote protein closure, which forces acCoA in an elongated form, pushing the substrate toward the opposite end of the substrate-binding pocket. This movement places the tails of the polyamine and acCoA directly under the active site residues (E49, Y199 and E56, Y207 in NATA1 and NATA2, respectively) for transfer of the acetyl moiety. Due to its length, spermine is likely to protrude out of the catalytic pocket in the closed form, as seen for the human SSAT1 bound to BE333 (PDB 2B4B). Conversely, our NATA1Δ structure bound to CoA and ornithine shows that ornithine can be completely captured in the enclosed binding site, similarly to moss SSAT bound to CoA and lysine (PDB 7ZKT) (Figure 2d,e).

2.4 | NATA2 is more heat stable than NATA1

Our results so far showed that NATA1 and NATA2 were structurally and catalytically very similar. To identify distinguishing features between the paralogues, we used differential scanning fluorimetry (DSF) to assess the stability of the purified *E. coli*–produced proteins.

FIGURE 2 Structural conformations from NATA1Δ and NATA2Δ crystal structures. (a) Superimposition of NATA1Δ (gray and cyan) and NATA2Δ (yellow) dimers. The plant-specific extension is shown in red. The CoA bound to NATA1Δ is shown as a stick model with carbons colored in pink. The structure on the right is rotated 90° along the x-axis. (b) Superimposition of apo-NATA2Δ (dark green), adopting the open conformation, onto the closed structure of NATA2Δ (yellow) bound to HEPES and acCoA (both shown as stick model). The carbon atoms of acCoA and HEPES are colored in pink and gray. Helices are shown as cylinders. Right figure shows the front view, as obtained by two orthogonal 90° rotations. (c) Electrostatic surface of apo-NATA2Δ (left, open conformation) and NATA2Δ bound to HEPES and acCoA (right, closed conformation). Structures are roughly placed in the orientation of (a), right panel, but slightly rotated around the Y axis to better show the changes in the open and closed conformations. (d) Top: Zoom view of the open NATA2Δ structure bound to spermine (green stick model). The two chains of NATA2Δ are shown in yellow and cyan. The side chains involved in binding to spermine are highlighted. Bottom: 2Fo-Fc omit map of spermine contoured to 1σ. (e) Top: Zoom view of NATA1Δ bound to ornithine (green stick) and CoA (pink stick). The two protein chains are shown in gray and cyan; involved side chains are highlighted. Bottom: 2Fo-Fc omit map of ornithine contoured to 1σ.

1469896x, 2026, 12, Downloaded from https://onlinelibrary.wiley.com/doi/10.1002/pro.70828 by Portail BibCNRS INSB, Wiley Online Library on [06/11/2026]. See the Terms and Conditions (https://onlinelibrary.wiley.com/terms-and-conditions) on Wiley Online Library for rules of use; OA articles are governed by the applicable Creative Commons License

With a melting temperature *Tm* of 42.5 ± 0.7°C, apo NATA1Δ was markedly less stable than apo NATA2Δ (*Tm* = 66.5 ± 0.5°C). The addition of 50 μM acCoA increased the *Tm* of NATA1Δ by 10°C, whereas acCoA only marginally stabilized NATA2Δ (Figure 3a and Table S3). The difference in stabilization was not caused by differences in binding energy, as both enzymes bound acCoA with a dissociation constant K_d of approximately 10 μM and similar entropy-dominated thermodynamics (Figure S3a,b). The presence of substrates did not lead to a significant increase in T_m for either enzyme (Figure S4a,b and Table S4). In agreement with its T_m, the ability of NATA1Δ to acetylate spermine declined at temperatures above 30°C, with a total loss of activity at 45°C. Conversely, the NATA2Δ activity on ornithine increased until 45°C (Figure 3b). As a result, the substrate preference profile of NATA2Δ at 45°C resembled that of NATA1Δ at 25°C, including ornithine (Figure 3c,d). Hence, at elevated temperature, NATA2 recovers the activity loss of NATA1.

To probe if the increased heat stability of NATA2 correlates with gene expression, we used previously described Arabidopsis knockout lines for *NATA2* (Salk_092319; *nata2*) (Lou et al. 2016). Quantitative RT-PCR revealed that NATA2 transcript levels increased within 2 h of exposure to 37°C (Figure 3e, left panel), in agreement with previous data (Kilian et al. 2007; Schmid et al. 2005; Waese et al. 2017). These results are consistent with enhanced expression of NATA2 under heat stress, supporting that the increased heat stability of NATA2 has physiological relevance.

To investigate the molecular basis for the difference in thermal stability, we searched for notable differences between the 76% sequence-identical paralogues. The most prominent difference occurs in the center of the dimer, close to the substrate-binding site, where NATA1 residues V75, Q146, and V181 are substituted in NATA2 by larger and/or more hydrophobic residues (F82, P154, and Y189, respectively) (Figure 3f). Their importance in stabilizing NATA2 is supported by stability calculations using FOLDX (Schymkowitz et al. 2005): Using the NATA2Δ apo structure as a template, the NATA2 sequence had a 23-kJ lower calculated energy than the NATA1 sequence. The in silico triple mutant increased or lowered the calculated energy for NATA1Δ and NATA2Δ, respectively, by more than 10 kJ (Figure S4c). In agreement, the recombinantly produced F82V, P154Q, and Y189V triple mutation decreased the NATA2Δ T_m by 10°C for the apo form and increased the stabilizing effect of acCoA significantly, akin to wild-type NATA1Δ. The NATA1Δ V75F/Q146P/V181Y mutant decreased the stabilizing effect of acCoA (from 10 to 6.5°C) but failed to increase the *Tm* of the mutant protein (Figure S4d and Table S3). We conclude that these three amino acid positions have a significant role in determining the protein stability. However, the three residues are insufficient to fully recapitulate the *Tm* differences, which, consequently, may result from the ensemble of minor changes across the protein fold.

2.5 | The substrate-binding pocket of NATA1 and NATA2 can accommodate acidic compounds

During our structural analysis we noted that the stereochemistry of the substrate-binding pocket of NATA1/2 differs markedly from the animal SSATs. In NATA1 and NATA2, the back of the substrate-binding pocket is formed by two arginines (R183/R214 in NATA1 and R191/R222 in NATA2), one from each molecule of the dimer. These residues project their side chains toward the non-acetylated end of the bound substrate (Figure 4a). This di-arginine motif is also found in moss SSAT and the bacterial SSATs (e.g., PDB 7ZHC, 2FE7). In the human form, this site is less positively charged. Consequently, the substrate-binding pocket of plant SSAT/NATAs more closely resembles that of bacterial enzymes than that of their animal counterparts.

Given that polyamines are positively charged, the presence of a di-arginine motif at the distal end of the substrate-binding site is unexpected, as this arrangement appears better suited to accommodate substrates terminating with acidic moieties. In support of this suggestion, in the open apo-NATA2 crystal structure (PDB 8RMZ) the di-arginine motif coordinates a sulfate ion derived from the crystallization solution (Figure S5a). Likewise, in our NATA2Δ structure bound to di-CoA (PDB 8XJH), the di-arginine motif coordinates the diphosphate moiety of a second CoA. This interaction likely underlies the capture of this second, presumably non-physiological CoA and its disulfate linkage to the CoA occupying the canonical binding site (Figure S5b), a ligand also present, but not discussed, in the Arabidopsis NATA2 structure deposited as PDB 7OVV.

Further evidence for the affinity of this site for acidic ligands comes from NATA1Δ and NATA2Δ structures obtained from crystals grown with 100 mM HEPES in the well solution. In these crystals, a HEPES molecule occupies the substrate-binding site despite the presence of substrate in the crystallization solution. In both structures, the di-arginine side chains coordinate the negatively charged sulfate moiety of HEPES. HEPES is further stabilized by additional hydrophobic and hydrogen bonds (Figures 4a and S5c), suggesting that HEPES is a potent inhibitor. Supporting this interpretation, the acetyl group of acCoA was absent in NATA1Δ crystals, where HEPES was added after the substrate, suggesting that acetyl transfer occurred before the addition of HEPES. In contrast, in NATA2Δ crystals, where HEPES was added before the substrate, the acetyl group of acCoA remains intact, inferring that HEPES has blocked substrate acetylation (Figure S5c).

1469896x, 2026, 12, Downloaded from https://onlinelibrary.wiley.com/doi/10.1002/pro.70828 by Portail BibCNRS INSB, Wiley Online Library on [06/11/2026]. See the Terms and Conditions (https://onlinelibrary.wiley.com/terms-and-conditions) on Wiley Online Library for rules of use; OA articles are governed by the applicable Creative Commons License

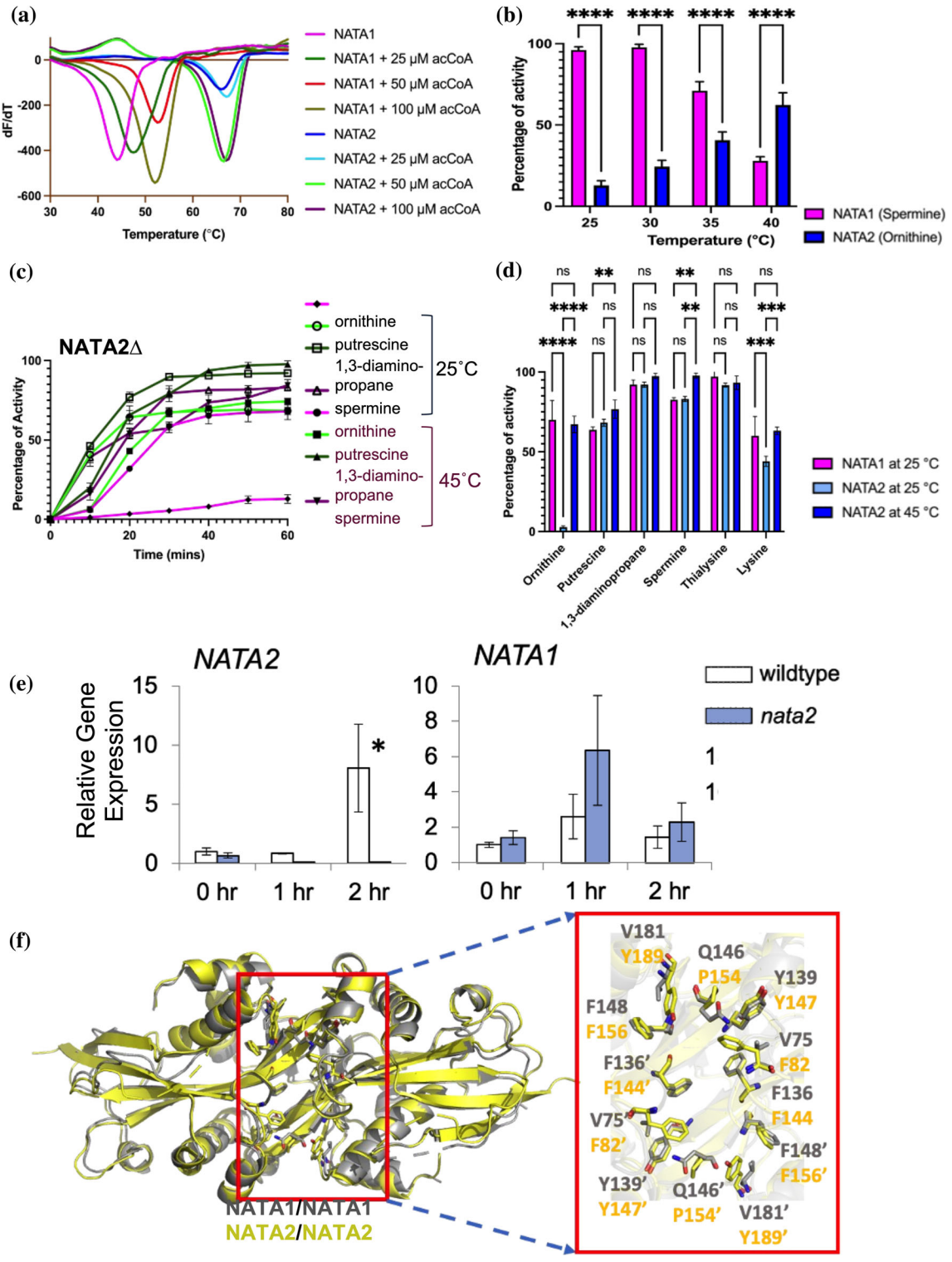
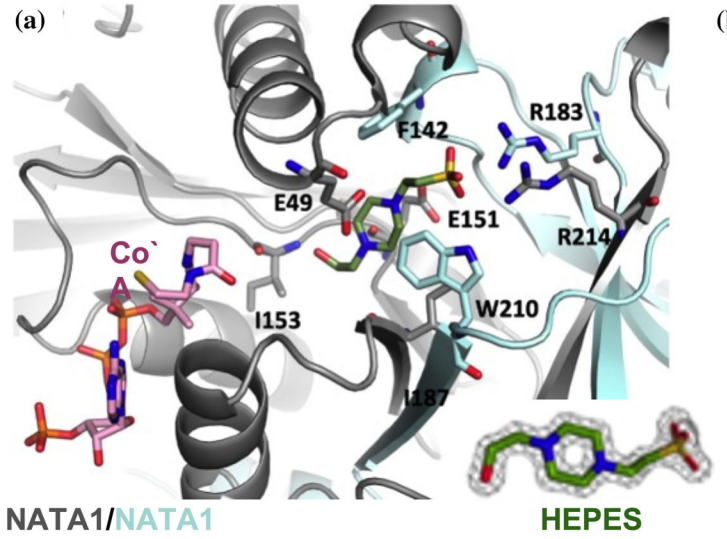
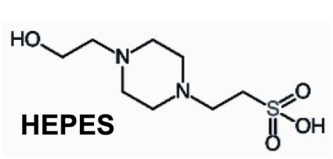
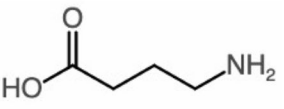


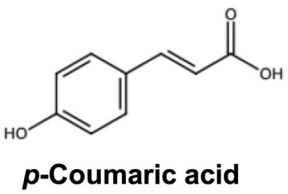
FIGURE 3 Heat stability of NATA1Δ and NATA2Δ and effect of temperature on catalysis. (a) Stability of NATA1Δ and NATA2Δ assayed by DSF in the presence of different concentrations of acCoA, measured in buffer *Tris8.5*. (b) Catalytic activity of NATA1Δ and NATA2Δ on spermine or ornithine at 25 and 45°C in buffer *Tris8.5*. Concentrations of substrate and acCoA were 5 and 0.5 mM, respectively. Protein concentrations were 3 μM. (c) Catalytic activity of NATA2Δ on its substrates at 25 and 45°C in buffer *Tris8.5*. Concentrations as in (a). (d) Endpoint histogram, based on data from (c). Data in panels (b–d) are presented as mean ± SEM from three independent replicates, and statistical comparisons were performed using two-way ANOVA followed by Tukey's multiple-comparison test (*$p < 0.05$; **$p < 0.01$; ***$p < 0.001$). (e) Altered heat stress and defense responses in *nata*mutants. Transcript abundance of NATA2 (left panel) and NATA1 (right panel), in wild type and *nata2* mutant seedlings, 0, 1, and 2 h after heat stress at 37°C. Gene expression was measured by quantitative RT-PCR. Mean ± SE of $N = 6–12$. *$p < 0.05$, two tailed *t*-test. (f) Superimposition of NATA1Δ bound to HEPES and CoA (gray) and NATA2Δ bound to HEPES and acCoA (yellow). Zoom figure shows the central core residues identified as modulating the stability of the proteins.

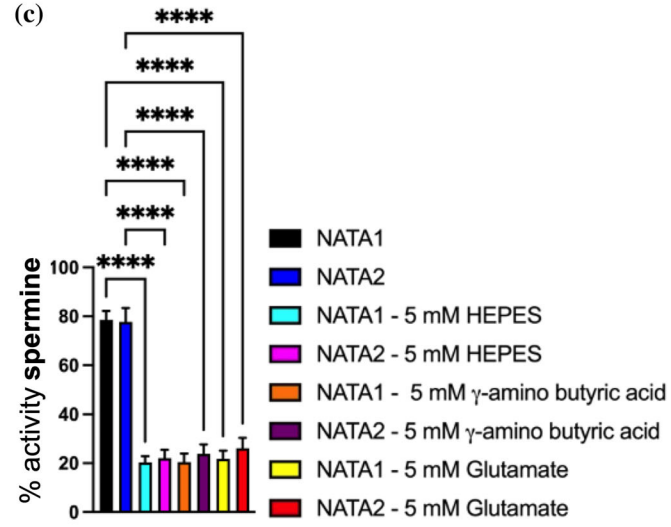
14698896x, 2026, 12, Downloaded from https://onlinelibrary.wiley.com/doi/10.1002/pro.70828 by Portail BibCNRS INSB, Wiley Online Library on [06/11/2026]. See the Terms and Conditions (https://onlinelibrary.wiley.com/terms-and-conditions) on Wiley Online Library for rules of use; OA articles are governed by the applicable Creative Commons License

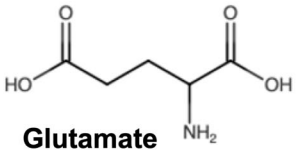


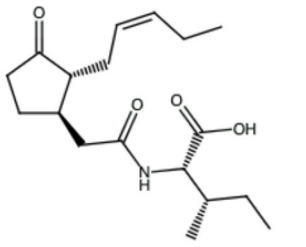


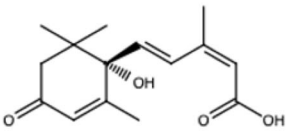












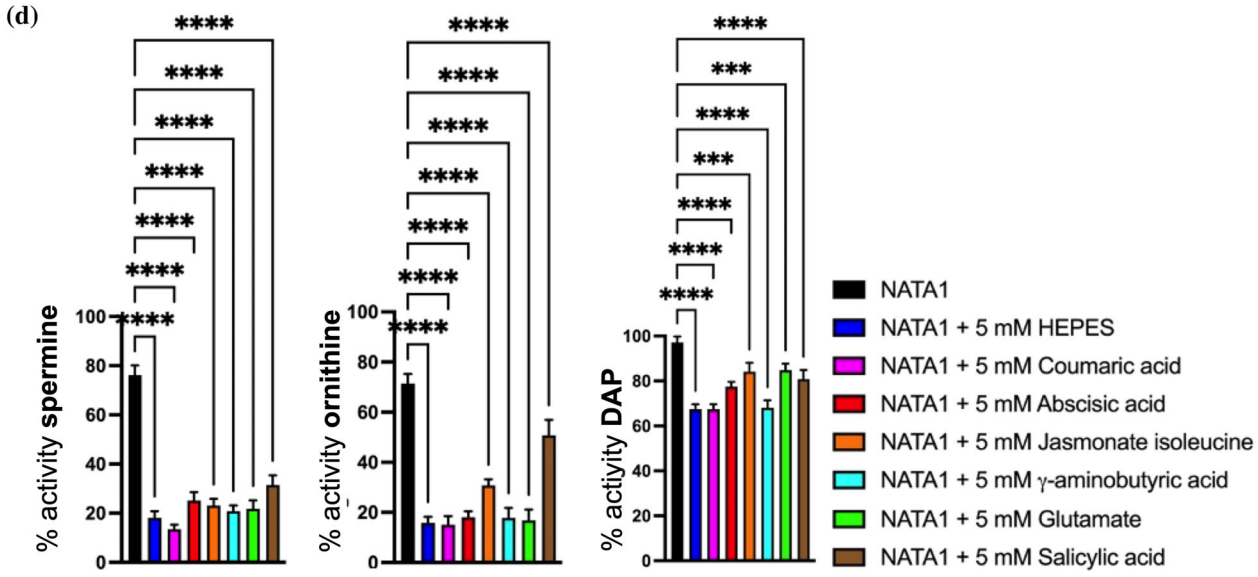


FIGURE 4 Legend on next page.

1469896x, 2026, 12, Downloaded from https://onlinelibrary.wiley.com/doi/10.1002/pro.70828 by Portail BibCNRS INSB, Wiley Online Library on [06/11/2026]. See the Terms and Conditions (https://onlinelibrary.wiley.com/terms-and-conditions) on Wiley Online Library for rules of use; OA articles are governed by the applicable Creative Commons License

Crystallization trials in the absence of HEPES allowed us to obtain a structure of NATA1Δ in the presence of CoA and ornithine. In this structure, the NATA1 di-arginine motif coordinates the acidic group of ornithine. The N-δ of ornithine was placed between the β-mercaptoethylamine group of CoA and the catalytic residues E49 and Y199, suggesting that this structure positions ornithine and CoA as in the active complex (Figure 2e). The position of ornithine in closed NATA1Δ corresponds to the position of lysine in moss SSAT (PDB 7ZKT), which also has a di-arginine motif (Figure S5d).

Given that compounds terminating in a negative charge match the NATA1/2 substrate-binding site, it is intriguing that the positively charged diaminopropane, spermine and putrescine are better substrates than ornithine, as reflected by their *Kcat*/*Km* (Table 2). Despite spermine having a lower *Km* than ornithine, our attempts to co-crystallize spermine and CoA with NATA1 or NATA2 in their closed protein conformation were unsuccessful. To explore potential binding modes, we employed AlphaFold3, which accurately recapitulated the positioning of CoA and ornithine in the closed NATA1 structure (Figure S6a). For spermine, AlphaFold3 predicted two distinct conformations. When modeled in the context of (ac)CoA-bound NATA1, the spermine tail was predicted to exit the active-site tunnel above the di-arginine motif. In contrast, in (ac)CoA-bound NATA2, the spermine tail was predicted to extend into the protein core, below the di-arginine motif (Figure S6b). These models indicate that spermine can, in principle, be accommodated within the closed active site. However, whether either (or both) of these conformations are biologically relevant remains to be established experimentally.

2.6 | Acidic endogenous metabolites modulate NATA catalytic activity

Our results showed that HEPES fitted the NATA1/2 substrate pockets well, and inhibited polyamine acetylation in vitro (Figure 4a). Indeed, in our in vitro acetylation assays, 5 mM HEPES reduced spermine acetylation by both NATA1Δ and NATA2Δ by about 80% (Figure 4b). We therefore hypothesized that endogenous acidic metabolites of comparable size might similarly inhibit NATA activity by competing with polyamines. To test this possibility, we selected a panel of biologically relevant plant metabolites with suitable size and charge properties, including γ-aminobutyric acid (GABA), glutamate, abscisic acid, salicylic acid, *p*-coumaric acid, and jasmonate-isoleucine. AlphaFold3 modeling predicted that all compounds could bind in the active site in the presence of CoA, with their acidic groups coordinated by the di-arginine motif (Figure S6c–h).

Experimental validation supported these predictions. In initial assays, 5 mM GABA or glutamate inhibited spermine acetylation by NATA1Δ and NATA2Δ as potently as HEPES (Figure 4b). We then examined this effect more systematically by testing 5 mM of each compound on NATA1Δ-mediated acetylation of spermine, ornithine, and 1,3-diaminopropane. All compounds reduced spermine and ornithine acetylation by 70–80%, comparable to HEPES, with the exception of salicylic acid that inhibited ornithine acetylation only by approximately 50% (Figure 4d). In contrast, inhibition of 1,3-diaminopropane acetylation was markedly weaker, ranging from less than 20% (for jasmonate-isoleucine and glutamate) to just over 30% (HEPES, *p*-coumaric acid, and GABA) (Figure 4d). These results demonstrate that endogenous acidic metabolites can potently and selectively inhibit NATA in vitro.

Given these shared inhibitory effects, we next asked whether the compounds might act synergistically. To test this possibility, we prepared a cocktail containing equal concentrations of glutamate, coumaric acid, abscisic acid, and GABA. In combination, only ∼60 μM of each compound (total ∼250 μM) was sufficient to significantly reduce the acetylation of spermine and thialysine by both NATA1 and NATA2 (Figure 5a). We further explored the cocktail effect by preparing a mixture of metabolites expected to co-exist in the Arabidopsis cytosol (i.e., glutamate, coumaric acid, salicylic acid, and jasmonate-isoleucine) at relative ratios approximating those observed under stress conditions (1:0.5:0.12:0.05). Starting from concentrations of 4, 2, 0.48, and 0.04 mM, respectively, this cocktail inhibited the NATA1-catalyzed acetylation of spermine, ornithine, and thialysine by approximately 80%. Inhibition of NATA1 remained significant even when concentrations were reduced to 63, 32, 7.5, and 0.63 μM, respectively. Consistent with our earlier findings, this mixture showed markedly lower activity toward 1,3-diaminopropane. Importantly, glutamate alone inhibited the acetylation of spermine and thialysine substantially less than the cocktail at the same glutamate concentration, confirming a

FIGURE 4 Inhibitors of NATA activity. (a) NATA1Δ bound to HEPES (olive green stick) and CoA (pink stick). The di-arginines coordinate the HEPES sulfate group. The catalytic E56 hydrogen-bonds with nitrogen N1 of HEPES, the backbones of E159 and D160 form hydrogen bonds with N4 and O8 of HEPES, and W218 and F150 form hydrophobic interactions with HEPES. Protein chains are shown in gray and cyan, and involved side chains are highlighted. Bottom: 2Fo-Fc omit map of HEPES. The omit map is contoured at 1σ. (b) Chemical structures of HEPES and endogenous metabolites used in the activity assays. (c) Catalytic activity of NATA1Δ and NATA2Δ on spermine in the presence of acidic compounds. (d) Catalytic activity of NATA1Δ against its substrates (from top to bottom: 1,3 diaminopropane, spermine, ornithine), in the presence of HEPES and 5 mM acidic endogenous metabolites. Data in panels (c, d) are shown as mean ± SEM from three independent replicates, and statistical comparisons were performed using a one-way ANOVA (*$p < 0.05$; **$p < 0.01$; ***$p < 0.001$).

1469896x, 2026, 12, Downloaded from https://onlinelibrary.wiley.com/doi/10.1002/pro.70828 by Portail BibCNRS INSB, Wiley Online Library on [06/11/2026]. See the Terms and Conditions (https://onlinelibrary.wiley.com/terms-and-conditions) on Wiley Online Library for rules of use; OA articles are governed by the applicable Creative Commons License

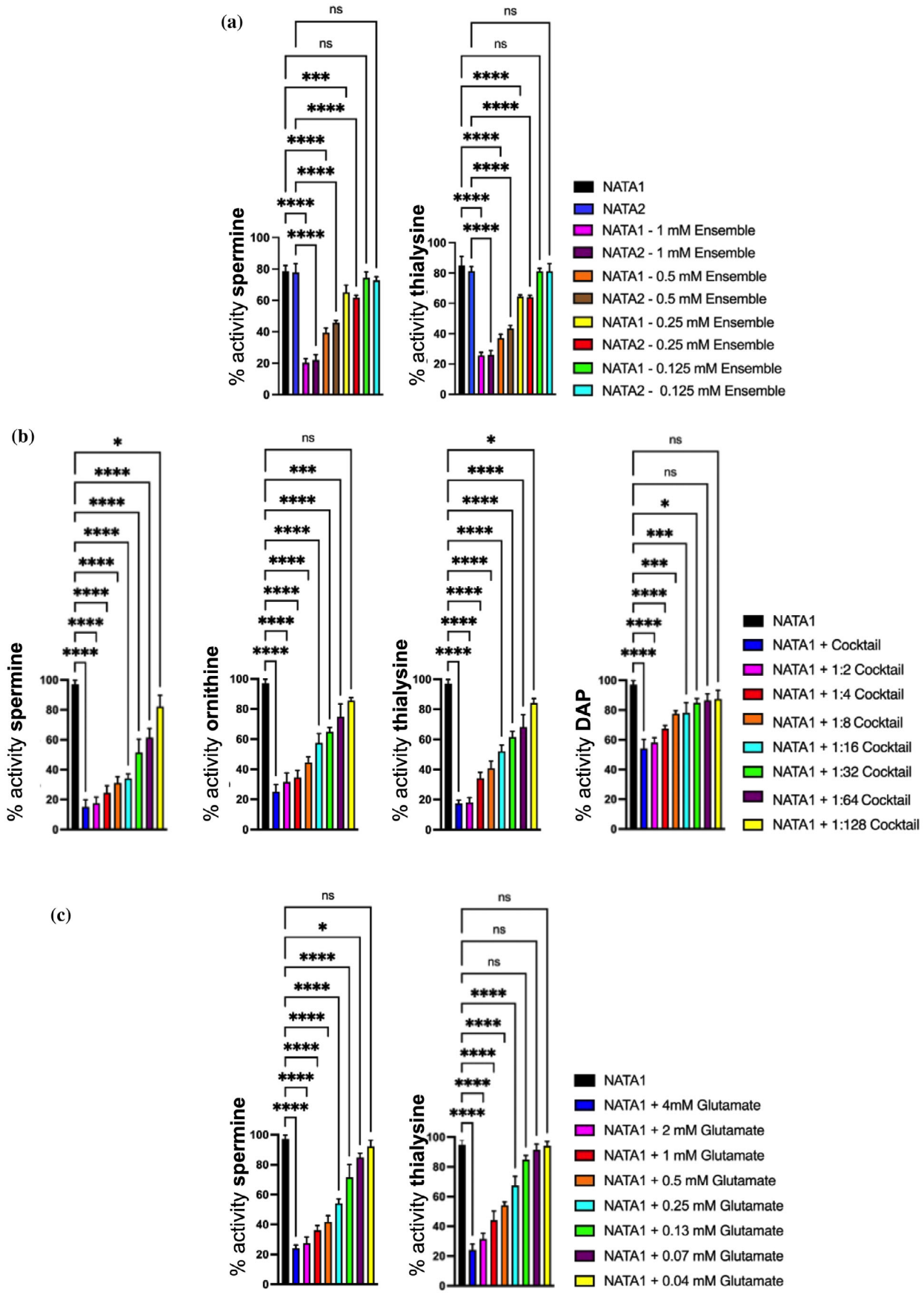


FIGURE 5 Legend on next page.

1469896x, 2026, 12, Downloaded from https://onlinelibrary.wiley.com/doi/10.1002/pro.70828 by Portail BibCNRS INSB, Wiley Online Library on [06/11/2026]. See the Terms and Conditions (https://onlinelibrary.wiley.com/terms-and-conditions) on Wiley Online Library for rules of use; OA articles are governed by the applicable Creative Commons License

synergistic mode of action (Figure 5b). For example, at 0.25 mM, glutamate alone inhibited acetylation of spermine and thialysine by 46 ± 3% and 32 ± 6%, respectively, whereas the cocktail achieved 66 ± 3% and 63 ± 4% inhibition (Figures 5c and S7 and Table S5).

Collectively, these results demonstrate that combinations of stress-associated metabolites, at physiologically relevant concentrations, can cooperatively attenuate NATA activity in vitro.

2.7 | Pockets in the NATA active site may allosterically influence catalysis

Even in the closed state, NATA1 and NATA2 retain large cavities near the di-arginine motif that were not occupied by co-crystallized compounds. In the NATA2Δ structure with HEPES and acCoA (PDB 8XJF), this pocket contains a glycerol molecule, likely from the cryoprotectant (Figure 6a). Glycerol was absent in the corresponding NATA1Δ structure despite similar conditions, suggesting slight differences in pocket size. Comparable cavities were observed in NATA orthologues from *P. patens*, which also bound glycerol. Additionally, an ethanediol molecule was present in *P. patens* (Figure 6a and Table S1). These structures suggested that the cavities adjacent to the NATA substrate binding can capture small molecules.

We tested the influence of 10% ethanediol, glycerol, and hexylene glycol on the acetylation of 1,3-diaminopropane, spermine, and ornithine by NATA1Δ (Figure 6b,c). Glycerol and hexylene glycol showed no effects on spermine and ornithine, and only mildly inhibited acetylation of 1,3-diaminopropane. This result was reassuring considering that 10–20% glycerol is frequently used in SSAT reactions and protein buffers (e.g., see Kuninger et al., 2007; Lou et al. 2016; Toleman et al., 2004). The absence of a marked effect of these compounds also supported the specificity, at least in vitro, of the strong inhibition observed through the acidic compounds. However, ethanediol significantly inhibited NATA1Δ activity for spermine and 1,3-diaminopropane (Figure 6c).

3 | DISCUSSION

In this study, we investigated the functional differences and regulation of Arabidopsis NATA1 and NATA2. By determining eight structures of NATA1 and NATA2, we gained detailed insights into the conformational transitions associated with substrate binding and catalysis. We confirmed that the plant-specific 35-residue insertion is partially structured in the Arabidopsis SSATs, adding an extra strand to the central β-sheet. Although the role of this insertion is still uncertain, our observation of a crystal contact-promoted rearrangement in this region raises the possibility that it functions as a ligand binding site.

The functional distinction between the two Arabidopsis NATA paralogues has remained unclear. In our analyses, NATA1 and NATA2 displayed highly similar catalytic properties, structures, and ligand interactions in vitro. However, NATA2 exhibited markedly greater thermal stability. Consistent with a biological relevance of this difference, NATA2, but not NATA1, was strongly upregulated under heat stress in seedlings. These observations suggest that NATA2 compensates for NATA1 loss under heat stress. Although the catalytic profiles of both NATA paralogues were highly similar, the low acetylation rate of ornithine by NATA2 at 25°C suggests functional differences that could explain the benefits of the NATA gene duplication and specification.

The overexpression of NATA1 and NATA2 under stress is intriguing, as their action lowers the concentration of polyamines, which have a protective role under stress (Gill and Tuteja 2010; Jang et al. 2012; Takahashi and Kakehi 2010). In view of this regulatory conundrum, it is interesting that our data suggest a metabolite-level autoregulatory mechanism that selectively attenuates some aspects of NATA activity under stress (Figure 7). This proposed mechanism hinges on stereochemical features of the NATA active site, including a di-arginine motif, that render the active site sufficiently permissive to catalyze polyamine acetylation while also allowing inhibition by acidic competitors. The serendipitous observation that HEPES binds tightly to this pocket and strongly inhibits catalysis led us to identify several endogenous plant metabolites (coumaric acid, abscisic acid, jasmonate-isoleucine, GABA, and glutamate) that similarly inhibited substrate acetylation. These molecules share key features with HEPES, including a central hydrophobic region and a negatively charged moiety. AlphaFold3 modeling supports the hypothesis that they bind in a comparable manner to HEPES, thereby blocking substrate access. Importantly, inhibition was substrate-selective in vitro. Although these

FIGURE 5 Combinatorial effects of inhibitors on NATA activity. (a) Catalytic activity of NATA1Δ against its substrates (spermine and thialysine), in the presence of increasing concentrations of a 1:1:1:1 mix of coumaric acid, abscisic acid, GABA, and glutamate. (b) Catalytic activity of NATA1Δ against the substrates spermine, ornithine, thialysine, and 1,3-diaminopropane in the presence of varying concentrations of a defined metabolite cocktail (glutamate, 4 mM; coumaric acid, 2 mM; salicylic acid, 0.48 mM; jasmonoyl-isoleucine, 0.04 mM). (c) Catalytic activity of NATA1Δ toward the substrates spermine and thialysine in the presence of varying concentrations of glutamate. The measurements in (a–c) were carried out in buffer *Tris8.5* at 25°C. Data in panels (a–c) are shown as mean ± SEM from three independent replicates, and statistical comparisons were performed using a one-way ANOVA (*$p < 0.05$; **$p < 0.01$; ***$p < 0.001$; ns, nonsignificant).

1469896x, 2026, 12, Downloaded from https://onlinelibrary.wiley.com/doi/10.1002/pro.70828 by Portail BibCNRS INSB, Wiley Online Library on [06/11/2026]. See the Terms and Conditions (https://onlinelibrary.wiley.com/terms-and-conditions) on Wiley Online Library for rules of use; OA articles are governed by the applicable Creative Commons License

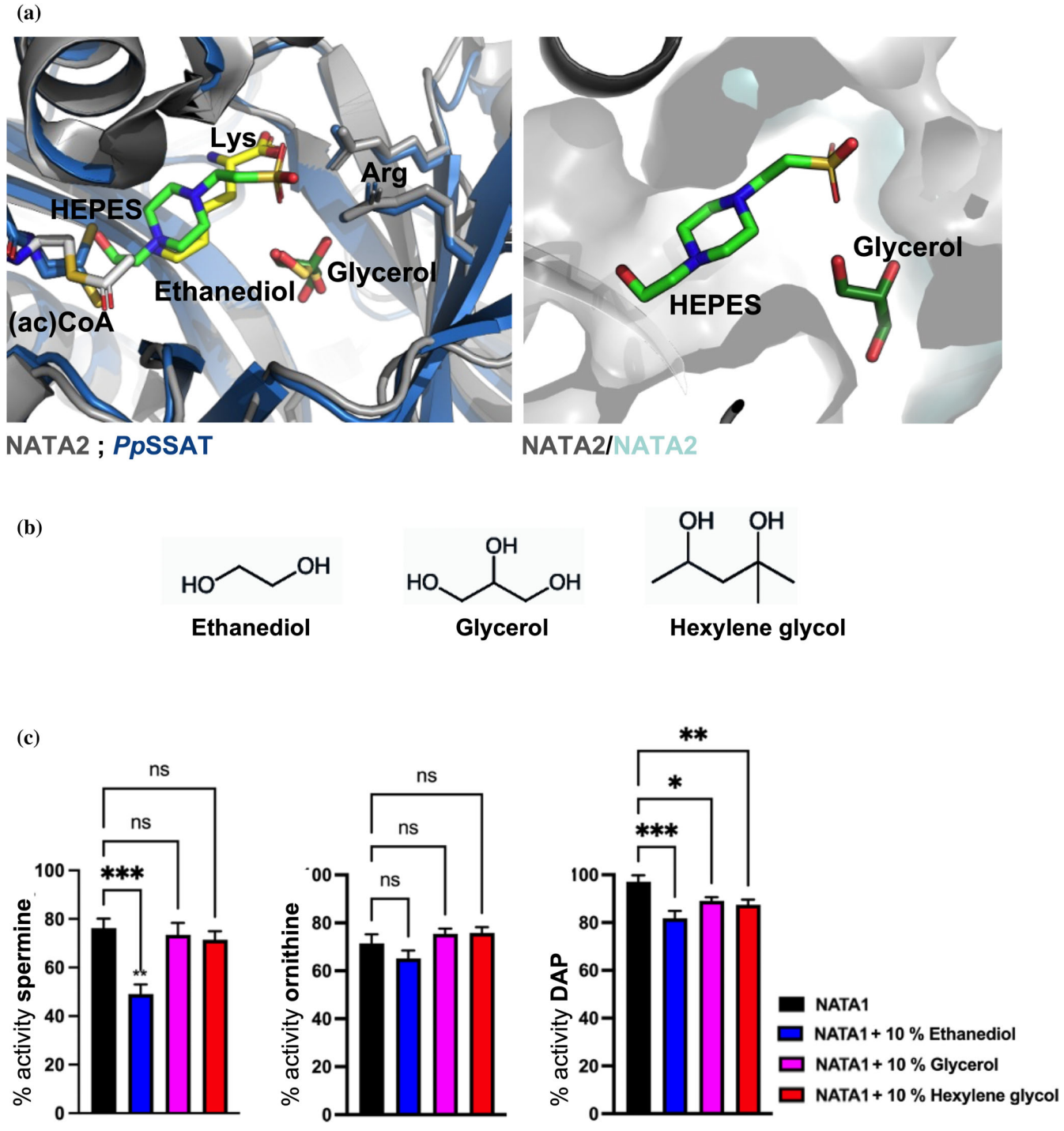


FIGURE 6 Modulators of NATA1 activity. (a) Left: Superimposition of the structures of NATA2Δ (gray) bound to HEPES (stick model with green carbons) and acCoA (light gray carbons) taken from PDB 8XJF, and of *Pp*SSAT (blue) bound to lysine (yellow) and CoA (blue), taken from PDB 7ZKT. Ethanediol (carbons in dark yellow; from PDB 8XJF) and glycerol (carbons in dark green; from PDB 7ZKT) are shown. Right: Zoom into NATA2Δ (gray and cyan) bound to HEPES (green) and glycerol (yellow), with transparent protein surfaces. Structure taken from PDB 8XJF. (b) Chemical structure of the compounds used in the activity assays. (c) Catalytic activity of NATA1Δ against its substrates in the presence of ethanediol, glycerol, and hexylene glycol in buffer *Tris8.5* at 25°C. Data are shown as mean ± SEM from three independent replicates, and statistical comparisons were performed using a one-way ANOVA (*$p < 0.05$; **$p < 0.01$; ***$p < 0.001$, and ns = not significant).

metabolites impaired acetylation of spermine and ornithine, the conversion of the smaller substrate 1,3-diaminopropane was only mildly affected. This suggests that inhibition reflects steric and electrostatic competition within the binding pocket rather than uniform catalytic suppression. Importantly, we showed that the inhibitory effects of different stress-related acidic metabolites can combine,

14698896x, 2026, 12, Downloaded from https://onlinelibrary.wiley.com/doi/10.1002/pro.70828 by Portail BibCNRS INSB, Wiley Online Library on [06/11/2026]. See the Terms and Conditions (https://onlinelibrary.wiley.com/terms-and-conditions) on Wiley Online Library for rules of use; OA articles are governed by the applicable Creative Commons License

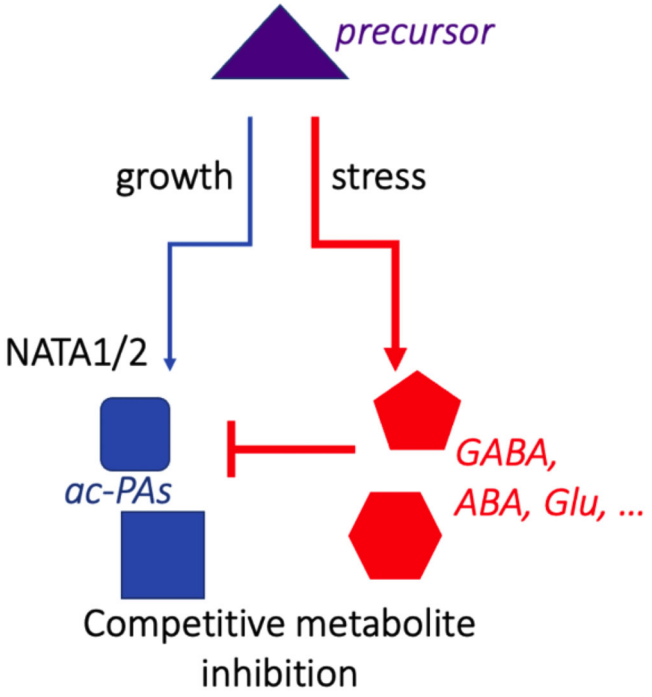


FIGURE 7 Schematic drawing illustrating the proposed autoregulation through competitive metabolite-ensemble inhibition. Conceptual drawing for NATA1/2 control by metabolites that reflect the cellular state. Blue: Under good growth conditions, NATA1/2 can acetylate the pool of polyamines to maintain homeostasis. Red: Acidic metabolites produced under stress conditions can directly and substrate-specifically inhibit NATA1/2, thus increasing the polyamine concentrations in ways that are favorable for the stressed plant.

forming a cocktail whose apparent inhibition level corresponds to the sum of the individual compounds.

It is notable that strong in vitro inhibition occurred at cocktail concentrations that are within the biological range of the metabolites under stress conditions. GABA and glutamate can reach millimolar concentrations in Arabidopsis. Although GABA is largely found in the plant vacuole, glutamate is abundant in the cytosol and nucleus (Koffler et al. 2011; Lou et al. 2016), where it could modulate NATA activity. Both metabolites have protective functions that increase the tolerance of plants to abiotic and biotic stress (Guo et al. 2023; Hasan et al. 2021; Li et al. 2021; Priya et al. 2019; Qiu et al. 2020; Sita and Kumar 2020). Coumaric acid contributes to pathogen defense. It is found primarily in the cytosol and apoplast and can exceed concentrations of 0.1 mM under stress in Arabidopsis (Liu et al. 2022; Macoy et al. 2015). Finally, the phytohormones abscisic acid and jasmonoyl-isoleucine regulate plant responses to drought, salinity, and wounding. Although present at lower concentrations than GABA and glutamate, their levels increase substantially under stress to 10–30 μM (Suza and Staswick 2008; Thurow et al. 2020), and NATA1 is among the most strongly jasmonate-induced genes in Arabidopsis (Adio et al. 2011). Given the chemical diversity of the compounds that showed an inhibitory effect in vitro, it is plausible that other acidic metabolites contribute to this ensemble-based regulation *in planta*. Our analysis also indicates that ethanediol can influence NATA catalysis by occupying a cavity adjacent to the active site. While the physiological relevance of this observation warrants further investigation, it should be taken into account when designing buffers for in vitro analyses.

In conclusion, our research elucidates the substrate turnover mechanism of plant SSATs/NATAs and identifies NATA2 as a paralogue that gains importance under heat stress. Our findings propose the hypothesis that NATA1 and NATA2 have evolved substrate-binding pockets that integrate metabolic signals into enzyme regulation. Under stress, the accumulation of acidic metabolites would inhibit polyamine acetylation, thereby preserving pools of protective polyamines. Notably, this inhibition would spare the acetylation of diaminopropane, whose modified form may itself support stress tolerance (Jammes et al. 2014). This selective, metabolite-mediated regulation hypothesis suggests a mechanistic framework for dynamic control of polyamine homeostasis during plant stress responses.

4 | METHODS

4.1 | Cloning, expression, and purification of NATA 1/2

N-terminally truncated NATA1 (19–228, NATA1Δ) and NATA2 (30–236, NATA2Δ) as well as the full-length NATA2 from Arabidopsis were cloned to the pGEX6P-1 expression vector (GE Healthcare). The plasmids were then transformed into Rosetta 2 (DE3) cells for expression. Cells producing the two truncated forms were grown in LB medium containing ampicillin (100 μg/mL) and chloramphenicol (35 μg/mL) at 37°C until an OD_{600} of 0.6. Protein expression was induced by adding 150 μM isopropyl β-D-1-thiogalactopyranoside (IPTG), and the cultures were incubated at 16°C overnight. For the full-length production, cells were grown in Terrific Broth medium supplemented with 200 mg/L carbenicillin and 30 mg/L chloramphenicol. Protein expression was induced at OD_{600} of 0.8 by adding 100 μM IPTG, and the cells were cultured at 18°C, overnight. Further affinity purification steps were followed as previously reported by Shahul Hameed and Siodmak et al. (2022;2023). After GST cleavage, the eluted proteins were purified on a HiLoad16/60 Superdex 200 prep-grade gel filtration column (GE Healthcare) using a buffer containing 20 mM Tris (pH 7.5), 150 mM NaCl, and 3 mM DTT. Protein purity was evaluated using SDS-PAGE. The purified NATA1Δ and NATA2Δ as well as the full-length NATA2 were

14698896x, 2026, 12, Downloaded from https://onlinelibrary.wiley.com/doi/10.1002/pro.70828 by Portail BibCNRS INSB, Wiley Online Library on [06/11/2026]. See the Terms and Conditions (https://onlinelibrary.wiley.com/terms-and-conditions) on Wiley Online Library for rules of use; OA articles are governed by the applicable Creative Commons License

concentrated to 10, 4, and to 5.2 mg/mL, respectively, and stored at −80°C.

4.2 | Crystallization and structure determination

NATA1Δ and NATA2Δ were preincubated with 2 mM acCoA (Roche) and 5 mM of ligands (purchased from Sigma) such as ornithine, spermine, and γ-aminobutyric acid. The protein complexes were then subjected to the sitting drop vapor diffusion method for crystallization screening using commercially available sparse matrix screens (Hampton research and Molecular dimensions). NATA1Δ crystals were obtained in the reservoir solutions containing 0.2M magnesium chloride hexahydrate, 0.1M HEPES pH 7.0, 20% w/v PEG 6000, and 0.2M ammonium sulfate, 0.1M Tris pH 8.5, 12% w/v PEG 8000. NATA2Δ crystals were obtained in the reservoir solution containing 0.2M sodium citrate tribasic dihydrate, 0.1M Tris pH 8.5, 30% v/v PEG 400, and 0.2M potassium thiocyanate, 0.1M Bis-Tris propane pH 7.5, 20% w/v PEG 3350, and 0.2M lithium chloride, 0.1M HEPES pH 7.0, 20% w/v PEG 6000. The crystals appeared after 7 days at 23°C. Apo NATA2 (full-length) crystals were obtained in the reservoir solution containing 0.2M ammonium sulfate, 0.1M Na-citrate pH 5.6, 15% v/v PEG 4000. As crystals were only identified after more than 4 weeks, a partial proteolysis of the flexible *N*-terminal residues 1–19 cannot be excluded. For data collection, 25% glycerol was used as a cryo-protectant and the crystals were flash-cooled in liquid nitrogen. Data were collected at 100 K at the beamlines PROXIMA 1 and PROXIMA 2A at the SOLEIL Synchrotron (France), using EIGER X 16M and EIGER X 9M detectors, respectively (Proposal numbers 20191181, 20191767, 20200610, 20201179, 20210195, 20210932, 20230217). The data were processed using either the "XDS made easier" pipeline (Legrand et al. 2019) or autoPROC (www.globalphasing.com) including STARANISO (Vonrhein et al. 2011). Initial phases were determined using human thialysine acetyltransferase (SSAT2) structure (PDB: 2BEI) as a search model for molecular replacement using Balbes or Phaser. The structures were manually inspected and corrected using Coot and refined using either Phenix Refine or BUSTER-2.10.4 (Blanc et al. 2004) using TLS group and NCS restraints (Table S2). The figures were drawn with PyMOL.

4.3 | Thermal shift assay

The thermal stability of NATA1Δ and NATA2Δ in the presence and absence of different ligands and cofactors was determined using thermal unfolding profiles. All assays were carried out at a final protein concentration of 10 μM, in a buffer containing 50 mM Tris–HCl pH 8.5, 150 mM NaCl, and with Sypro Orange dye (Invitrogen) at a 2× final concentration. Thermal denaturation temperatures were obtained in a CFX96 touch real-time thermal cycler (Bio-Rad) with an optical reaction module by ramping the temperature between 20 and 95°C at 1°C per minute, and fluorescence acquisition through the channel. Data were analyzed with CFX Manager Software V3.0 (Bio-Rad) and plotted using PRISM version 9.0 (www.graphpad.com).

4.4 | Acetyltransferase activity using DTNB assay

The catalytic activity of NATA1Δ and NATA2Δ was measured spectrophotometrically on a Pherastar plate reader (BMG Labtech) at 25°C using a dithiobis-(2-nitrobenzoic acid) (DTNB) assay. The assay was carried out using various ligands following the previously reported work by Bělíček et al. (2023). The substrate screening was made in 50 mM Tris–HCl pH 8.5, 150 mM NaCl, using 0.5 acCoA, 5 mM substrate, and 0.5 mM DTNB. Ligand titration assays were performed using defined concentration schemes depending on the compound. Most test compounds were assayed at a single concentration of 5 mM. Enzymatic activity was expressed as percentage conversion relative to a CoA standard. Complete conversion of 500 μM acetyl-CoA to CoA was considered 100% activity, corresponding to the signal obtained from a 500 μM CoA standard. The percentage activity of each sample was calculated based on the amount of CoA produced relative to this reference value. For selected ligands used in ensemble analyses (coumaric acid, abscisic acid, γ-aminobutyric acid [GABA], and glutamate), stock solutions were prepared at 1 mM and diluted to the indicated concentrations. Glutamate titration experiments were carried out using a serial dilution range from 4 mM to 40 μM. For combinatorial ("cocktail") assays, glutamate (4 mM), coumaric acid (2 mM), salicylic acid (0.48 mM), and jasmonoyl-isoleucine (JA-Ile; 0.04 mM) were mixed and serially diluted, and activity measurements were performed across the resulting concentration range. Enzymatic activity assays were further carried out in the presence of 10% hexylene glycol (MPD), ethanediol, and glycerol under the conditions described above with the respective substrates. The data were plotted using PRISM version 9.0 (www.graphpad.com).

4.5 | Isothermal titration calorimetry

NATA1Δ and NATA2Δ were dialyzed and degassed in the isothermal titration calorimetry (ITC) buffer (20 mM Tris pH 7.5, 150 mM NaCl, 3 mM DTT). AcCoA (Roche) and CoA (Sigma) were dissolved in the identical buffer. For the titrations, 20 μM of NATA1Δ and

1469896x, 2026, 12, Downloaded from https://onlinelibrary.wiley.com/doi/10.1002/pro.70828 by Portail BibCNRS INSB, Wiley Online Library on [06/11/2026]. See the Terms and Conditions (https://onlinelibrary.wiley.com/terms-and-conditions) on Wiley Online Library for rules of use; OA articles are governed by the applicable Creative Commons License

NATA2Δ were placed in the cell, and 350 μM of acCoA and CoA were loaded in the syringe. Titrations were performed at 25°C with an initial injection of 0.4 μL, followed by 18 injections of 2 μL. ITC experiments were performed on ITC200 (Malvern Panalytical, UK). Data analysis was performed and figures prepared using MicroCal Origin 7 software.

4.6 | Plants and growth conditions

Seeds of wild-type Columbia-0 Arabidopsis and *nata2* (Salk_092319; Alonso et al. 2003) were obtained from the Arabidopsis Biological Resource Center (www.arabidopsis.org). Plants were grown in Cornell mix (by weight 56% peat moss, 35% vermiculite, 4% lime, 4% Osmocoat slow-release fertilizer [Scotts, Marysville, OH], and 1% Unimix [Scotts]) in 20 × 40-cm nursery flats in Conviron growth chambers with a photosynthetic photon flux density of 200 mmol m^{-1} s^{-1} and a 16:8 h day:night photoperiod, at 23°C with a 50% relative humidity. For experiments carried out at elevated temperature, a chamber set to identical conditions except for a 28°C temperature was used.

4.7 | Quantitative PCR

Relative transcript abundances of *NATA2* (At2g39020) and *NATA1* (At2G39030) were analyzed and compared by qRT-PCR using actin (At3g18780) as an endogenous control as described in Lou et al. (2016). Gene-specific primers were designed using Primer-Blast (www.ncbi.nlm.nih.gov/tools/primer-blast/) and listed in Table S6. Rosette leaf samples were ground in liquid nitrogen and total RNA was extracted using the SV total RNA isolation system (Promega, www.promega.com). After quantification with a Nanodrop system (www.nanodrop.com), 1 μg of total RNA was reverse transcribed using SMART® MMLV Reverse Transcriptase (Clontech, www.clontech.com) using oligo$(dT)_{15}$ primers. Following cDNA synthesis, the samples were diluted in nuclease free water and used for qRT-PCR reactions with the SYBR® Green PCR master mix (Applied Biosystems, www.appliedbiosystems.com) using an Applied Biosystems 7900HT Instrument. Each reaction was carried out with the following conditions: 95°C for 10 min, followed by 40 cycles of 95°C for 15 s, 60°C for 15 s, and 72°C for 15 s, and final extension at 72°C for 2 min. The C_T values were quantified and analyzed according to the standard curve method.

AUTHOR CONTRIBUTIONS

Umar F. Shahul Hameed: Conceptualization; methodology; software; data curation; investigation; validation; formal analysis; visualization; project administration; resources. **Yann-Ru Lou:** Investigation; validation; formal analysis; methodology; visualization. **Aleczander Young:** Methodology; validation. **Jian Yan:** Visualization. **Francisco J Guzmán-Vega:** Software. **Ekaterina Aleksenko:** Methodology; protein production. **Huaiyuan Ma:** Software. **Pierre Briozzo:** Methodology; software; validation. **Solange Moréra:** Methodology; software; validation; formal analysis; visualization; writing – review and editing. **Georg Jander:** Conceptualization; methodology; writing – review and editing. **Stefan T. Arold:** Conceptualization; methodology; software; data curation; investigation; validation; formal analysis; supervision; funding acquisition; visualization; project administration; resources; writing – original draft; writing – review and editing.

ACKNOWLEDGMENTS

This research was funded by US National Science Foundation awards 1121788 and 1022017 to GJ and by King Abdullah University of Science and Technology (KAUST) through the baseline fund to STA (BAS/1/1056-01-01). This work benefited from the I2BC crystallization platforms supported by FRISBI ANR-10-INSB-05-01. P. Briozzo thanks Fonds Saint-Michel (1, rue Lhuillier 75015 Paris, France) and Institut du Cancer et d'Immunogénétique (ICIG, Hôpital Paul-Brousse, 14, avenue Paul-Vaillant-Couturier, 94807 Villejuif, France) for financial support. We acknowledge SOLEIL for provision of synchrotron radiation facilities and would like to thank A. Thompson, P. Montaville, P. Legrand, S. Sirigu, M. Savko, and B. Shepard for assistance in using the beamlines PROXIMA 1 and PROXIMA 2A (Proposal IDs: 20191767, 20191181, 20200610, 20201179, 20210195, 20210932, and 20230217). For computer time, this research used the resources of the KAUST Supercomputing Laboratory, and experimental research was supported by the Bioscience Core Lab and the Imaging and Characterization Core Lab at King Abdullah University of Science & Technology (KAUST) in Thuwal, Saudi Arabia. We thank Navid Mohaved for assistance with mass spectrometry assays and Yiping Qi for providing the *nata2* TALEN knockout line described by Christian et al. 2013. E. Aleksenko thanks V. Gaudin and J. Leung for supervision, Y. Sulio for his help, and the University of Paris-Saclay for her PhD fellowship. During the preparation of this work the authors used Copilot in order to improve the language in some passages. After using this tool/service, the authors reviewed and edited the content as needed and take full responsibility for the content of the publication.

CONFLICT OF INTEREST STATEMENT

The authors declare no conflicts of interest.

DATA AVAILABILITY STATEMENT

The data that support the findings of this study are openly available in Protein Data Bank at https://www.

1469896x, 2026, 12, Downloaded from https://onlinelibrary.wiley.com/doi/10.1002/pro.70828 by Portail BibCNRS INSB, Wiley Online Library on [06/11/2026]. See the Terms and Conditions (https://onlinelibrary.wiley.com/terms-and-conditions) on Wiley Online Library for rules of use; OA articles are governed by the applicable Creative Commons License

rcsb.org/, reference numbers 8RMZ, 8XJ9, 8XJB, 8XJF, 8XJH, 8XBN, 8XJ5, and 8XBP.

ORCID

Umar F. Shahul Hameed https://orcid.org/0000-0002-0552-7149
Yann-Ru Lou https://orcid.org/0000-0002-4716-4323
Aleczander Young https://orcid.org/0000-0002-6610-7981
Jian Yan https://orcid.org/0000-0002-8215-8084
Ekaterina Aleksenko https://orcid.org/0009-0008-2814-3245
Huaiyuan Ma https://orcid.org/0009-0004-0929-0646
Solange Moréra https://orcid.org/0000-0001-7781-0448
Georg Jander https://orcid.org/0000-0002-9675-934X
Stefan T. Arold https://orcid.org/0000-0001-5278-0668

REFERENCES

Adio AM, Casteel CL, De Vos M, Kim JH, Joshi V, Li B, et al. Biosynthesis and defensive function of *N* Δ-Acetylornithine, a Jasmonate-induced Arabidopsis metabolite. Plant Cell. 2011;23:3303–18.

Alonso JM, Stepanova AN, Leisse TJ, Kim CJ, Chen H, Shinn P, et al. Genome-wide insertional mutagenesis of *Arabidopsis thaliana*. Science. 2003;301:653–7.

Bagni N, Tassoni A. Biosynthesis, oxidation and conjugation of aliphatic polyamines in higher plants. Amino Acids. 2001;20:301–17.

Bělíček J, Ľuptáková E, Kopečný D, Frömmel J, Vigouroux A, Ćavar Zeljković S, et al. Biochemical and structural basis of polyamine, lysine and ornithine acetylation catalyzed by spermine/spermidine *N* -acetyl transferase in moss and maize. Plant J. 2023;114:482–98.

Bewley MC, Graziano V, Jiang J, Matz E, Studier FW, Pegg AE, et al. Structures of wild-type and mutant human spermidine/spermine N^1-acetyltransferase, a potential therapeutic drug target. Proc Natl Acad Sci U S A. 2006;103:2063–8.

Blanc E, Roversi P, Vonrhein C, Flensburg C, Lea SM, Bricogne G. Refinement of severely incomplete structures with maximum likelihood in *BUSTER–TNT*. Acta Crystallogr D Biol Crystallogr. 2004;60:2210–21.

Christian M, Qi Y, Zhang Y, Voytas DF. Targeted mutagenesis of *Arabidopsis thaliana* using engineered TAL effector nucleases. G3 Genes|Genomes|Genetics. 2013;3:1697–705.

Coleman CS, Hu G, Pegg AE. Putrescine biosynthesis in mammalian tissues. Biochem J. 2004;379:849–55.

Della Ragione F, Pegg AE. Effect of analogues of 5′-methylthioadenosine on cellular metabolism. Inactivation of *S* -adenosylhomocysteine hydrolase by 5′-isobutylthioadenosine. Biochem J. 1983;210:429–35.

Evans PT, Malmberg RL. Do polyamines have roles in plant development? Annu Rev Plant Physiol Plant Mol Biol. 1989;40:235–69.

Fliniaux O. Altered nitrogen metabolism associated with de-differentiated suspension cultures derived from root cultures of *Datura stramonium* studied by heteronuclear multiple bond coherence (HMBC) NMR spectroscopy. J Exp Bot. 2004;55:1053–60.

Galston AW, Kaur-Sawhney R, Altabella T, Tiburcio AF. Plant polyamines in reproductive activity and response to abiotic stress. Botanica Acta. 1997;110:197–207.

Galston AW, Sawhney RK. Polyamines in plant physiology. Plant Physiol. 1990;94:406–10.

Gill SS, Tuteja N. Polyamines and abiotic stress tolerance in plants. Plant Signal Behav. 2010;5:26–33.

Guo Z, Gong J, Luo S, Zuo Y, Shen Y. Role of gamma-aminobutyric acid in plant defense response. Metabolites. 2023;13:741.

Han BW, Bingman CA, Wesenberg GE, Phillips GN. Crystal structure of *Homo sapiens* thialysine N^{ϵ}-acetyltransferase (HsSSAT2) in complex with acetyl coenzyme A. Proteins. 2006;64:288–93.

Hanfrey C, Sommer S, Mayer MJ, Burtin D, Michael AJ. Arabidopsis polyamine biosynthesis: absence of ornithine decarboxylase and the mechanism of arginine decarboxylase activity. Plant J. 2001;27:551–60.

Hasan MM, Alabdallah NM, Alharbi BM, Waseem M, Yao G, Liu X-D, et al. GABA: a key player in drought stress resistance in plants. Int J Mol Sci. 2021;22:10136.

Hegde SS, Chandler J, Vetting MW, Yu M, Blanchard JS. Mechanistic and structural analysis of human spermidine/Spermine N^1-acetyltransferase. Biochemistry. 2007;46:7187–95.

Hennion F, Bouchereau A, Gauthier C, Hermant M, Vernon P, Prinzing A. Variation in amine composition in plant species: how it integrates macroevolutionary and environmental signals. Am J Botany. 2012;99:36–45.

Jammes F, Leonhardt N, Tran D, Bousserouel H, Véry A, Renou J, et al. Acetylated 1,3-diaminopropane antagonizes abscisic acid-mediated stomatal closing in Arabidopsis. Plant J. 2014;79:322–33.

Jang SJ, Wi SJ, Choi YJ, An G, Park KY. Increased polyamine biosynthesis enhances stress tolerance by preventing the accumulation of reactive oxygen species: T-DNA mutational analysis of *Oryza sativa* lysine decarboxylase-like protein 1. Mol Cells. 2012;34:251–62.

Kamada-Nobusada T, Hayashi M, Fukazawa M, Sakakibara H, Nishimura M. A putative peroxisomal polyamine oxidase, AtPAO4, is involved in polyamine catabolism in *Arabidopsis thaliana*. Plant Cell Physiol. 2008;49:1272–82.

Kilian J, Whitehead D, Horak J, Wanke D, Weinl S, Batistic O, et al. The AtGenExpress global stress expression data set: protocols, evaluation and model data analysis of UV-B light, drought and cold stress responses. Plant J. 2007;50:347–63.

Kim DW, Watanabe K, Murayama C, Izawa S, Niitsu M, Michael AJ, et al. Polyamine oxidase5 regulates Arabidopsis growth through thermospermine oxidase activity. Plant Physiol. 2014;165:1575–90.

Koffler BE, Maier R, Zechmann B. Subcellular distribution of glutathione precursors in *Arabidopsis thaliana*. J Integr Plant Biol. 2011;53:930–41.

Kuninger D, Lundblad J, Semirale A, Rotwein P. A non-isotopic in vitro assay for histone acetylation. J Biotechnol. 2007;131(3):253–60. https://doi.org/10.1016/j.jbiotec.2007.07.498

Kusano M, Fukushima A, Arita M, Jonsson P, Moritz T, Kobayashi M, et al. Unbiased characterization of genotype-dependent metabolic regulations by metabolomic approach in *Arabidopsis thaliana*. BMC Syst Biol. 2007;1:53.

Kusano T, Berberich T, Tateda C, Takahashi Y. Polyamines: essential factors for growth and survival. Planta. 2008;228:367–81.

Legrand P, Soleilproxima, Aishima J, CV-GPhL. legrandp/xdsme: March 2019 version working with the latest XDS version (January 26, 2018). 2019 https://doi.org/10.5281/ZENODO.837885

Li L, Dou N, Zhang H, Wu C. The versatile GABA in plants. Plant Signal Behav. 2021;16:1862565.

Liu S, Jiang J, Ma Z, Xiao M, Yang L, Tian B, et al. The role of hydroxycinnamic acid amide pathway in plant immunity. Front Plant Sci. 2022;13:922119.

Lou Y-R, Bor M, Yan J, Preuss AS, Jander G. Arabidopsis NATA1 acetylates putrescine and decreases defense-related hydrogen peroxide accumulation. Plant Physiol. 2016;171(2):1443–55. https://doi.org/10.1104/pp.16.00446

Macoy DM, Kim W-Y, Lee SY, Kim MG. Biotic stress related functions of hydroxycinnamic acid amide in plants. J Plant Biol. 2015;58:156–63.

1469896x, 2026, 12, Downloaded from https://onlinelibrary.wiley.com/doi/10.1002/pro.70828 by Portail BibCNRS INSB, Wiley Online Library on [06/11/2026]. See the Terms and Conditions (https://onlinelibrary.wiley.com/terms-and-conditions) on Wiley Online Library for rules of use; OA articles are governed by the applicable Creative Commons License

Mattioli R, Pascarella G, D'Incà R, Cona A, Angelini R, Morea V, et al. Arabidopsis N-acetyltransferase activity 2 preferentially acetylates 1,3-diaminopropane and thialysine. Plant Physiol Biochem. 2022;170:123–32.

Mesnard F, Azaroual N, Marty D, Fliniaux M-A, Robins RJ, Vermeersch G, et al. Use of 15N reverse gradient two-dimensional nuclear magnetic resonance spectroscopy to follow metabolic activity in Nicotiana plumbaginifolia cell-suspension cultures. Planta. 2000;210:446–53.

Montemayor EJ, Hoffman DW. The crystal structure of spermidine/spermine N^1-acetyltransferase in complex with spermine provides insights into substrate binding and catalysis. Biochemistry. 2008;47:9145–53.

Moschou PN, Wu J, Cona A, Tavladoraki P, Angelini R, Roubelakis-Angelakis KA. The polyamines and their catabolic products are significant players in the turnover of nitrogenous molecules in plants. J Exp Bot. 2012;63:5003–15.

Nahar K, Hasanuzzaman M, Rahman A, Alam MM, Mahmud J-A, Suzuki T, et al. Polyamines confer salt tolerance in mung bean (*Vigna radiata* L.) by reducing sodium uptake, improving nutrient homeostasis, antioxidant defense, and methylglyoxal detoxification systems. Front Plant Sci. 2016;7:1104.

Pegg AE. Spermidine/spermine-N^1-acetyltransferase: a key metabolic regulator. Am J Physiol Endocrinol Metabol. 2008;294:E995–E1010.

Priya M, Sharma L, Kaur R, Bindumadhava H, Nair RM, Siddique KHM, et al. GABA (γ-aminobutyric acid), as a thermoprotectant, to improve the reproductive function of heat-stressed mungbean plants. Sci Rep. 2019;9:7788.

Qiu X-M, Sun Y-Y, Ye X-Y, Li Z-G. Signaling role of glutamate in plants. Front Plant Sci. 2020;10:1743.

Regla-Márquez CF, Canto-Flick A, Avilés-Viñas SA, Valle-Gough RE, Pérez-Pastrana J, García-Villalobos FJ, et al. Cadaverine: a common polyamine in zygotic embryos and somatic embryos of the species *Capsicum chinense* Jacq. Plant Cell Tiss Organ Cult. 2016;124:253–64.

Rhee HJ, Kim E, Lee JK. Physiological polyamines: simple primordial stress molecules. J Cell Mol Med. 2007;11:685–703.

Sagor GHM, Inoue M, Kim DW, Kojima S, Niitsu M, Berberich T, et al. The polyamine oxidase from lycophyte *Selaginella lepidophylla* (SelPAO5), unlike that of angiosperms, back-converts thermospermine to norspermidine. FEBS Lett. 2015;589:3071–8.

Schmid M, Davison TS, Henz SR, Pape UJ, Demar M, Vingron M, et al. A gene expression map of Arabidopsis thaliana development. Nat Genet. 2005;37:501–6.

Schymkowitz J, Borg J, Stricher F, Nys R, Rousseau F, Serrano L. The FoldX web server: an online force field. Nucleic Acids Res. 2005;33:W382–8.

Sen S, Ghosh D, Mohapatra S. Modulation of polyamine biosynthesis in Arabidopsis thaliana by a drought mitigating *Pseudomonas putida* strain. Plant Physiol Biochem. 2018;129:180–8.

Shahul Hameed U, Haider I, Jamil M, Guo X, Zarban RA, Kim D, et al. Structural basis for specific inhibition of the highly sensitive ShHTL7 receptor. EMBO Rep. 2022;23:e54145.

Siodmak A, Shahul Hameed UF, Rayapuram N, Völz R, Boudsocq M, Alharbi S, et al. Essential role of the CD docking motif of MPK4 in plant immunity, growth, and development. New Phytol. 2023;239:1112–26.

Sita K, Kumar V. Role of gamma amino butyric acid (GABA) against abiotic stress tolerance in legumes: a review. Plant Physiol Rep. 2020;25:654–63.

Sobieszczuk-Nowicka E. Polyamine catabolism adds fuel to leaf senescence. Amino Acids. 2017;49:49–56.

Suza WP, Staswick PE. The role of JAR1 in Jasmonoyl-l-isoleucine production during Arabidopsis wound response. Planta. 2008;227:1221–32.

Takahashi T, Kakehi J-I. Polyamines: ubiquitous polycations with unique roles in growth and stress responses. Ann Bot. 2010;105:1–6.

Takahashi Y, Tahara M, Yamada Y, Mitsudomi Y, Koga K. Characterization of the polyamine biosynthetic pathways and salt stress response in *Brachypodium distachyon*. J Plant Growth Regul. 2018;37:625–34.

Tavladoraki P, Cona A, Angelini R. Copper-containing amine oxidases and FAD-dependent polyamine oxidases are key players in plant tissue differentiation and organ development. Front Plant Sci. 2016;7:824.

Tavladoraki P, Cona A, Federico R, Tempera G, Viceconte N, Saccoccio S, et al. Polyamine catabolism: target for antiproliferative therapies in animals and stress tolerance strategies in plants. Amino Acids. 2012;42:411–26.

Thurow C, Krischke M, Mueller MJ, Gatz C. Induction of jasmonoyl-isoleucine (JA-Ile)-dependent *JASMONATE ZIM-DOMAIN* (*JAZ*) genes in NaCl-treated *Arabidopsis thaliana* roots can occur at very low JA-Ile levels and in the absence of the JA/JA-Ile transporter JAT1/AtABCG16. Plants (Basel). 2020;9:1635.

Toleman C, Paterson AJ, Whisenhunt TR, Kudlow JE. Characterization of the histone acetyltransferase (HAT) domain of a Bifunctional protein with Activable O-GlcNAcase and HAT activities. J Biol Chem. 2004;279(51):53665–73. https://doi.org/10.1074/jbc.m410406200.

Vonrhein C, Flensburg C, Keller P, Sharff A, Smart O, Paciorek W, et al. Data processing and analysis with the *autoPROC* toolbox. Acta Crystallogr D Biol Crystallogr. 2011;67:293–302.

Waese J, Fan J, Pasha A, Yu H, Fucile G, Shi R, et al. ePlant: visualizing and exploring multiple levels of data for hypothesis generation in plant biology. Plant Cell. 2017;29:1806–21.

Wimalasekera R, Tebartz F, Scherer GFE. Polyamines, polyamine oxidases and nitric oxide in development, abiotic and biotic stresses. Plant Sci. 2011;181:593–603.

Xiang C, Ao Y-F, Höhne M, Bornscheuer UT. Shifting the pH optima of (R)-selective transaminases by protein engineering. Int J Mol Sci. 2022;23(23):15347.

Yoda H, Fujimura K, Takahashi H, Munemura I, Uchimiya H, Sano H. Polyamines as a common source of hydrogen peroxide in host- and nonhost hypersensitive response during pathogen infection. Plant Mol Biol. 2009;70:103–12.

Yoda H, Hiroi Y, Sano H. Polyamine oxidase is one of the key elements for oxidative burst to induce programmed cell death in tobacco cultured cells. Plant Physiol. 2006;142:193–206.

Zahedi K, Barone S, Soleimani M. Polyamines and their metabolism: from the maintenance of physiological homeostasis to the mediation of disease. Med Sci (Basel). 2022;10:38.

SUPPORTING INFORMATION

Additional supporting information can be found online in the Supporting Information section at the end of this article.

How to cite this article: Shahul Hameed UF, Lou Y-R, Young A, Yan J, Guzmán-Vega FJ, Aleksenko E, et al. Mechanism and regulation of Arabidopsis polyamine acetylation by NATA1 and NATA2. Protein Science. 2026;35(12):e70828. https://doi.org/10.1002/pro.70828

1469896x, 2026, 12, Downloaded from https://onlinelibrary.wiley.com/doi/10.1002/pro.70828 by Portail BibCNRS INSB, Wiley Online Library on [06/11/2026]. See the Terms and Conditions (https://onlinelibrary.wiley.com/terms-and-conditions) on Wiley Online Library for rules of use; OA articles are governed by the applicable Creative Commons License